BIOSYNTHESIS OF SELENIUM (Se) NANOPARTICLES AND THEIR USE AS CO-CATALYST FOR ZINC SULFIDE (ZnS) PHOTOCATALYSED DEGRADATION OF DYE

A Dissertation

Submitted in the partial fulfilment of requirement for the award of the

Degree of

Master of Technology

In

Environmental Science and Technology

Submitted by

Saniya Ahluwalia
(601301011)

Under the supervision of

Dr. N. Tejo Prakash
Professor
School of Energy & Environment

Dr. Bonamali Pal
Professor
School of Chemistry & Biochemistry

School of Energy and Environment
Thapar University
Patiala - 147004
Punjab, India

July, 2015

Declaration

I, hereby declare that the work presented in thesis entitled "***Biosynthesis of Selenium (Se) nanoparticles and their use as co-catalyst for Zinc Sulphide (ZnS) photocatalysed degradation of dye***" in fulfilment of the requirement for the award of the Degree of Master of Technology in Environmental Science and Technology, School of Energy and Environment, Thapar University, Patiala is an authentic record of my own work carried out under the supervision of Dr. N. Tejo Prakash (Professor, School of Energy and Environment) and Dr. Bonamali Pal (Professor and Head, School of Chemistry and Biochemistry), Thapar University, Patiala. The matter embodied in this thesis has not been submitted in part or full to any other university or institute for the award of any degree.

Saniya Ahluwalia

602301011

Place: Patiala

Date: July 15, 2015

Certificate

This is to certify that the thesis entitled "***Biosynthesis of Selenium (Se) nanoparticles and their use as co-catalyst for Zinc sulphide (ZnS) photocatalysed degradation of dye***", being submitted by Miss. Saniya Ahluwalia in partial fulfilment of the requirement for the award of Degree of Master of Technology in Environmental Science and Technology, School of Energy and Environment, Thapar University, Patiala, is a record of candidate's own work carried out by her under our supervision and guidance. The matter presented in this thesis has not been submitted in part or full for the award of any degree to any other University or Institute.

Supervisor

Dr. N. Tejo Prakash
Professor,
School of Energy and Environment,
Thapar University, Patiala

Dr. Bonamali Pal
Professor,
School of Chemistry and Biochemistry,
Thapar University, Patiala

Countersigned by

Dr. A.S. Reddy
Head,
School of Energy and Environment,
Thapar University, Patiala

Dr. S.S. Bhatia
Dean of Academic Affairs,
Thapar University, Patiala

Acknowledgements

Through this section of the thesis, I would like to convey my heartiest thanks to all those who supported and encouraged me in many ways throughout for the accomplishment of this project.

I would like to extend my sincerest gratitude to my supervisor, ***Dr. N. Tejo Prakash****, Professor, School of Energy and Environment, Thapar University, Patiala for giving me the valuable opportunity to work under his worthy guidance. He has been a source of inspiration and direction to me. It was his splendid supervision, support and unending patience that helped me in executing this task from its conception to completion.*

I take this opportunity to thank ***Dr. Bonamali Pal****, Professor, School of Chemistry and Biochemistry, Thapar University, Patiala for helping me with his immense knowledge, constructive ideas, critical and timely suggestions, effort, time and patience throughout my work.*

I would also like to acknowledge faculty of School of Energy and Environment, Thapar University, Patiala for their encouraging and supporting nature and specially ***Dr. A.S. Reddy****, Head, School of Energy and Environment, Thapar University, Patiala for allowing me to work on the project of my choice. I am also grateful to other staff members of School of Energy and Environment.*

Special thanks to ***Mr. Sumit Jaiswal****,* ***Mr. Bhupender Pal*** *and* ***Mr. Rayees Ahmad*** *for their kind assistance, cooperation and generous help whenever I needed. I have deep gratitude towards them for never turning down any query. I would also like to thank* ***Miss Noorpreet Dhanjal*** *and* ***Mr. Anirudh Sharma*** *for their timely help, support and encouragement.*

I would like to express my regards to my family for being source of inspiration, dedication and encouragement in my life. To them I dedicate my thesis. And I would also like to thank my friends who expressed their constant moral support, care and understanding towards me. Finally, praises and thanks to the almighty God, the most merciful and compassionate, for His blessings throughout my project work to complete it successfully.

Saniya Ahluwalia

Abstract

The work presented in this thesis outlines the importance of biosynthesized selenium nanoparticles (SeNPs) as co-catalysts for the enhancement of as-synthesized ZnS based photocatalysis. ZnS nanoparticles (ZnSNPs) were synthesized following reflux-condensation approach and examined for its potential to degrade a synthetic dye compound, methyl orange. To enhance the efficacy of ZnS, Se nanoparticles that were synthesized using biogenic approach were calcined with ZnS to generate Se-ZnS nanocomposites (Se-ZnSNCs). The as-synthesized SeNPs, ZnSNPs and the Se-ZnSNCs were characterized by UV-Vis spectroscopy, DLS, XRD and SEM-EDX. Amongst the nanomaterials tested, the Se-ZnSNCs showed higher degradation potential to the extent of 95% when compared to ZnSNPs (55%) and SeNPs (8.5%). Further, the influence of concentration of Se was significant with supplementation of Se by 1wt% which enhanced the photodegrading ability of nanocomposites by 95% when compared to 0.25, 0.5 and 2.0 wt% supplementation of Se during Se-ZnSNCs synthesis. The reaction followed pseudo first-order kinetics with an apparent rate constant k of 8.42×10^{-3} min^{-1}.

List of Contents

List of Figures

List of Tables

1. Introduction

The emerging field of nanoscience and nanotechnology has stimulated a great interest over the last few years due to its prospective impact on many areas such as energy, environment, healthcare, IT, electronics and space industries. Nanotechnology is of global interest because of its potential. Its potential lies in designing, characterizing and producing structures, devices and systems by controlling shape and size at the nanoscale, that is, a billionth of a meter (10^{-9} m). The objective of nanotechnology is to direct atoms and molecules to form desired material with novel functionality.

At the nanoscale, fundamental characteristics of a material like magnetic properties, band gap energy, melting point, thermal conductivity, etc can be controlled without altering its chemical composition [1]. This result in materials called nanoparticles (NPs) with changed physical, chemical and biological properties having fundamental and valuable properties as compared to properties of bulk matter. They show unique properties due to their size, structure and vastly increased surface-to-volume ratio, which open its new possibilities in many applications viz. renewable energy generation, solar cells, environment remediation, photocatalysis, superconductors, agriculture and food industry, skin care, drug delivery, antimicrobial activity, and many more [2].

Nanotechnological approaches are continually being studied to develop novel and cost effective measures for environmental remediation by detecting, preventing, controlling and removing pollutants which will lead to a cleaner and healthier environment. NPs are being used as potent adsorbents and catalysts for chemical or photochemical degradation of contaminants. Magnetic NPs like zerovalent iron are deployed to remove contaminants from soil and ground water by easing particle separation, semiconductor nanomaterials like TiO_2, ZnS, ZnO are extensively used for oxidative or reductive removal of organic pollutants and nanosized sensors hold promise for improved detection and tracking of contaminants in air and water [3, 4]. Overall, there are numerous promising environmental applications for nanotechnology. Much of the current research is focused on energy and water treatment technologies.

One such approach is *photocatalysis*, described as the acceleration of the rate of chemical reactions that may be oxidation or reduction in the presence of a catalyst by ultraviolet (UV) or visible light irradiation. In the frame of reference of history and research, in 1972,

Fujishima and Honda [5] discovered the photochemical splitting of water into hydrogen and oxygen in the presence of heterogeneous photocatalyst TiO_2. This outstanding invention lead to onset of photo induced redox reactions by using a variety of semiconductor catalyst materials.

Semiconductor NPs have been a subject of substantial interest because of their immense applications as a photocatalysts, photovoltaic devices, optical sensitizers, biomedical sensors, etc [6, 7]. Amongst the various photocatalysts being explored till date, ZnS is an important II-IV direct semiconductor material with a wide band gap i.e., 3.5-3.7 eV for cubic and 3.7–3.8 eV for hexagonal structure and high excition binding energy i.e. 40 meV [8]. This makes it suitable semiconductor material for variety of applications. One such application is heterogeneous photocatalysis for the degradation of organic dye pollutants. However, due to limitations in efficacy [9, 10] it is of importance to improve the photocatalytic efficiency of ZnSNPs.

However, many of the photo-catalysts do not work effectively just by themselves, but work in conjunction with some other promoters commonly known as "*co-catalysts*". Co-catalysts can be understood as the components that activate the catalyst or modify its action and make the catalytic process feasible. Many researches had improved the photocatalytic activity of TiO_2 by doping many transition metals like Fe, Cd, Ni, Cu, Zn, Ag, Au, B, etc. by different approaches, for example, the hydrothermal treatment [11], the spray pyrolysis deposition [12], the sol-gel method [13], magnetron cosputtering technique [14], and the electrochemical method [15]. Most of the these synthetic methods of doping are characteristic of complex reaction conditions such as the intense ultrasonication, the ultraviolet irradiation, the long aging process, the elevated reaction pressure and temperature, as well as the use of expensive metal salt solutions ($HAuCl_4$, $AgNO_3$, $PdCl_2$, H_2PtCl_6). Moreover, these methods are related with various problems including use of harmful chemical agents (hydrazine, surfactants) and production of hazardous commodities.

Many efforts have also been exploited to enhance ZnS based photocatalytic activity, such as doping ZnS with different metal ions such as Mn, Ni, Cu [16], Fe [17] by chemical precipitation and electrochemically coupling ZnS with narrow band gap semiconductor like Se [18]. As an effective alternative to robust and expensive chemical approach for doping ZnS, a promising move to reach this objective is to use biological resources in nature. One approach that shows immense potential is based on the biosynthesis of NPs using

microorganisms (a kind of bottom up approach) [19]. Microbial synthesis of NPs is a green chemistry approach that interconnects nanotechnology and microbial biotechnology.

Among various co-catalysts, elemental selenium (Se) possesses many unique physical and chemical properties. It is an n-type indirect semiconductor which exhibits good photoelectrical properties, optoelectronic properties, high photoconductivity (8×10^4 S/cm) and piezoelectricity, thermoelectricity and also catalytic activities towards oxidation reaction and organic-hydration [20-22]. Elemental selenium (Se) has narrow band gap of 1.85ev with relatively low melting point (~217°C), high refractive index and high reactivity making it leading suitable compound for carrying out chemical reactions.

We used as-synthesized ZnS nanoparticles impregnated with biogenic Se as co-catalysts to examine their efficacy to degrade a model dye compound, Methyl orange. Dyes are effective organic pollutants produced in large amount by many different industries, including the textile, paper, leather, cosmetic, pharmaceutical and food industries [23]. Many research groups have reported the photodegradation and mineralization of organic pollutants by heterogenous photocatalysis [24].

Thus, considering the need for the development of easy, reliable and an inexpensive approach for generation of Se-ZnS nanocomposites, wet impregnation method has been employed for the synthesis of Se-ZnSNCs in aqueous solution where ZnSNPs synthesized [25] and impregnated with Se nanoparticles so as to generate nanocomposites. A comparative study was carried out to evaluate the photocatalytic efficacy of as synthesized Se, ZnS and Se-ZnS NCs to degrade methyl orange and analyse the role of biogenically synthesized Se as a co-catalyst.

2. Review of Literature

2.1 Concept of nanomaterials

Nanotechnology is the study of process, control and consolidation of materials by one atom or by one molecule at the nanoscale level i.e. 10^{-9} m or one billionth of a meter. The term "nanotechnology" was framed in 1974 by the Japanese Scientist Norio Taniguchi in the conference paper "On the Basic Concept of 'Nano-Technology'" [26]. It is an interdisciplinary domain in which concepts and ideas derived from physics, chemistry, engineering, biology, material science, computer science, etc. are amalgamated to design materials or systems with unique properties. Materials or systems in the range of nanoscale exhibit novel and significantly improved physical, chemical and biological features, phenomena and processes which make them suitable for numerous applications.

Nanomaterials are being used in almost every field which includes energy, environment, electronics, optics, information technology, magnetics, materials development and healthcare [27, 28].

The unique properties of nanoparticles include surface (high surface to volume ratio) [29], quantum confinement [30], optical properties [31] and electrical properties [32]. In addition, features such as melting point [30], magnetic [33, 34] and mechanical properties [30] are significantly different from that of bulk materials.

2.2 Synthesis of nanoparticles

The synthesis of NPs may be divided into two major categories: a) *Bottom-up approach* in which synthesis is done by collecting individual atoms and b) *Top-down approach* where bulk material is subdivided into nanoscale dimensions [35]. Arrays of physical, chemical and biological methods have been formulated to synthesize NPs with a range of compositions, sizes and shapes. Fig. 1 outlines the various approaches for the synthesis of NPs.

However, physical methods have one main disadvantage of generating poor quality of products as compared to products synthesized by chemical methods. Chemical synthesis provides good control of size, shape, stability and the assembly of NPs by optimizing reaction conditions such as concentration, temperature and by incorporating capping agents (such as polymers), solvents and templates [36].

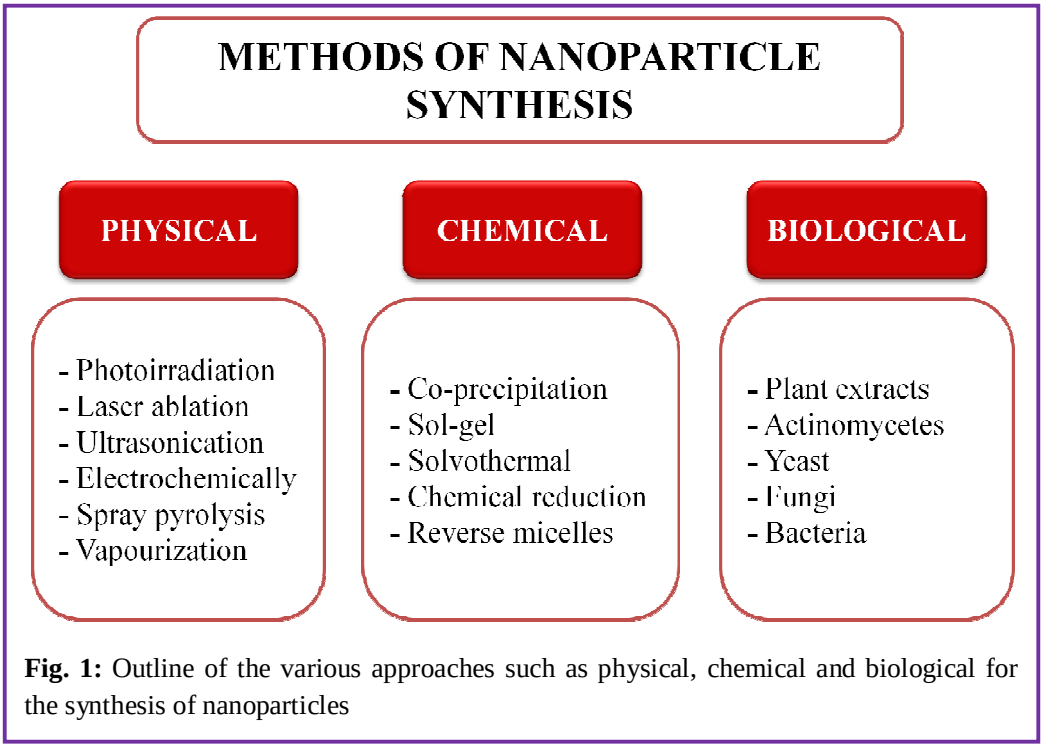

Fig. 1: Outline of the various approaches such as physical, chemical and biological for the synthesis of nanoparticles

With high pace of development in the field of nanotechnology, the new approaches for synthesis of nanomaterials have become essential. Although the physical and chemical methodologies have been used successfully to produce nanomaterials, these techniques are often tedious, hazardous and environmentally challenging. Furthermore, in addition to being an expensive approach, chemicals reagents used normally for NPs synthesis and stabilization are toxic and also lead to produce toxic by-products. Therefore, there is a growing concern to develop eco-friendly and sustainable methods for the synthesis of nanomaterials. In the following section, various biological methods for the synthesis of NPs have been illustrated.

2.3 Biological synthesis of nanoparticles

The use of biological means for synthesis of NPs is gaining greater attention as it is a green synthesis approach that interconnects nanotechnology and microbial biotechnology. These biological methods assist to remove ruthless processing conditions by allowing the synthesis at physiological pH, temperature, and at the same time, at negligible cost. Biological methods utilize nature's most valuable machines i.e. living cells for the synthesis of NPs. The following Fig. 2 depicts the scheme of synthesis of NPs by microorganisms.

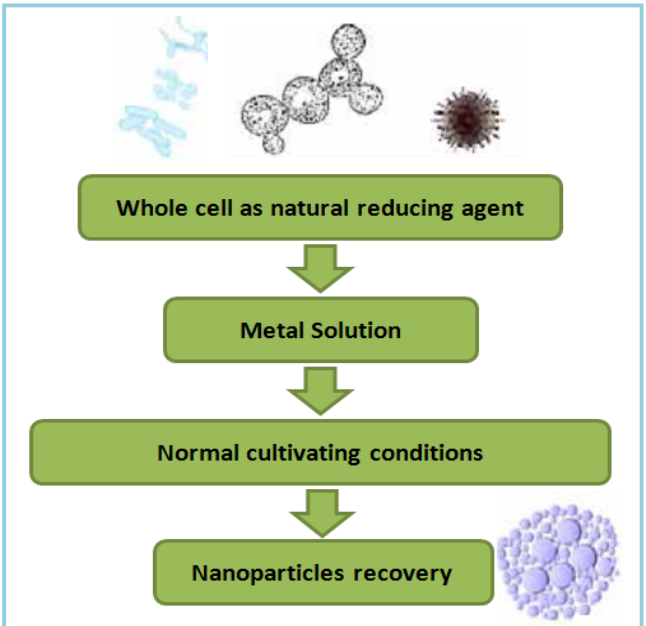

Fig. 2: Scheme of synthesis of nanoparticles by various microorganisms

This unique ability of microorganisms has been realized only recently when they were used for the bioremediation of toxic metal ions. Synthesis of inorganic NPs is feasible due to specific resistant mechanism offered by microorganisms against the high metal ion concentration such as modification in the solubility of metal ions, modification in redox state, discharging of metal ions by efflux pumps, formation of complexes with metal ions or extracellular precipitation of metal ions etc [37]. Thus, biosynthesis of NPs is considered to be a bottom-up approach, where during the synthesis the oxidation/reduction is the main reaction that occurs. Many biological systems, including plants [38-42], actinomycetes [43-46], yeast [47-51], fungi [52-57], and bacteria have the ability to transform inorganic metal ions into metal NPs via the reductive capacities of the proteins and metabolites present in these organisms.

2.4 Bacteria: Pioneering biomachines generating nanoparticles

Bacteria can be considered as living, eco-friendly nano-factories. They hold immense potential to synthesize various inorganic nanomaterials ranging from simple metals to more complex systems such as metal sulfides and metal oxides. Bacteria synthesize inorganic nanomaterials either intracellularly or extracellularly often in nanoscale dimensions with exquisite morphology. The synthesis takes place in response to detoxification of ions either by reduction or oxidation through various routes likely extracellular biomineralization,

biosorption, complexation, precipitation or intracellular bioaccumulation. Extracellular production of metal NPs has more commercial applications in various fields. Since the polydispersity is the major concern, it is important to optimize the conditions for monodispersity in a biological process. In case of intracellular production, the accumulated particles are of particular dimension with less polydispersity.

Naturally controlled biosynthesis of nanomaterials strive tight control over the size, shape and composition of NPs, therefore restricting the synthesis to limited number of NPs. But by the use of bacteria, induced biosynthesis of nanomaterials can be carried out by altering the parameters like temperature, pH, metal ion concentration, incubation time, etc., which offers great potential to synthesise wide range of nanomaterials [37]. Diverse varieties of bacteria have been reported to exhibit the potential to generate nanoparticles as means of dissimilatory metal reduction or to reduce toxicity [58].

Therefore, vast range of inorganic nanomaterials having properties identical to chemically and physically synthesized nanomaterials could be synthesized using bacteria due to their rich diversity and potential. Different size, shape and composition of the NPs can also be controlled by using them. Bacteria possess several advantages that make it most used microorganism for synthesis of nanomaterials [37].

- It is easy to culture them on a large scale. It has both intracellular as well as extracellular capacity to intake the reduction of metallic particles and rendering them to elemental state.
- Bacteria have unique nature to work. It's highly selective 'sieve-like' nature can absorb useful metals and reduce them into pure elemental form of NPs.
- All of the NPs can be produced at room temperature, highlighting how little energy is required for their synthesis by using bacteria as compared to other methods.
- Bacteria can act together to produce a large number of highly desirable metals in their wild-type forms; it is easy to see how synthetic biology could be used to take such diversity as a starting point and engineer bacteria for wider applications, such as contaminant identification/detoxification as well as the specific production of a NP from a mixture of substrates such as found in soil or water.

2.5 Biosynthesis of selenium nanoparticles (SeNPs)

Selenium has a complete biogeochemical cycle in nature, with microbial redox reactions leading both to and from all of its oxidation states to elemental state i.e. Se^0. A variety of microorganisms, such as bacteria and fungi, have been used to synthesise SeNPs of different size and morphology. Bacteria reduce the toxic, selenate and selenite oxoanions into non toxic elemental selenium which is insoluble in water under aerobic as well as anaerobic conditions. It is a simple process of detoxification of selenites/selenates to SeNPs in the forward reaction. Elemental selenium produced is stable product as the reverse reaction is too slow to produce Se compounds [59, 60].

Fast (forward reaction)

$$SeO_3^{2-}/SeO_4^{2-} \rightleftharpoons Se^0$$

Slow (backward reaction)

Different concentrations of Se were allowed to interact with different types of microbes. Appearance of red colour was taken as sign of reduction of SeO_3^{2-}/SeO_4^{2-} to Se^0 as shown in forward reaction above. This reaction process is time and concentration dependent. Over 16 different species of bacteria and Archaea have been found to reduce colourless selenate and selenite to red, amorphous or monoclinic allotropes of Se^0 i.e. elemental Se of different shape and size. They accumulate in spent medium or within the cell as bacteria reduce selenate or selenite to Se^0. Table 1 gives overview of various bacteria responsible for SeNPs synthesis.

Table 1: Various bacteria that synthesize SeNPs [60]

Bacterial sp.	**Substrate**
Bacillus mycoides	SeO_3^{2-}
Sulfurospirillum barnesii, Bacillus selenireducens	SeO_3^{2-}
Zooglea ramigera	SeO_3^{2-}, SeO_4^{2-}
Pseudomonas aeruginosa	SeO_3^{2-}
Pseudomonas alcaliphila	SeO_3^{2-}
Escherchia coli	SeO_3^{2-}
Duganella sp., Agrobacterium sp.	SeO_3^{2-}
Bacillus cereus	SeO_3^{2-}
Klebsiella pneumonia	Se_2Cl_2
Shewanella sp.	SeO_3^{2-}
Tetrathiobacter kashmirensis	SeO_3^{2-}
Enterobacter hormaeche	SeO_4^{2-}
Stenotrophomonas maltophilia	SeO_3^{2-}, SeO_4^{2-}
Ferrimonas futtsuensis, Selenihalanaerobacter shriftii	SeO_4^{2-}

2.6 Applications of SeNPs in environmental remediation

Research has been carried out considering SeNPs due to its unique properties and large inherent applications. Se is an indirect semiconductor which shows good nonlinear optical properties, photoelectrical properties, high photoconductivity, piezoelectric and thermoelectric responses, and low melting point and also has good catalytic activities towards organic hydration and oxidation reactions. With this potential, SeNPs have been exploited in many fields [61]. More recently, potential of SeNPs in the field of environmental remediation is being exploited. SeNPs have been shown to sequester elemental mercury released from mercury contaminated museum specimens [62].

Secondly, semiconductor NPs are well known for one of their properties i.e. photocatalysis. Se as one of the most important semiconductors is well exploited for its photovoltaic and optoelectronic properties. However, so limited findings have been reported on the photocatalytic activity of pristine SeNPs, with the exception of a few recent studies. Photocatalytic activity of Se NPs/NRs for degradation of methylene blue and congo red under UV light irradiation has been reported [63, 64]. Nath *et al.* [65] also reported photocatalytic degradation of methylene blue by Triton X-100 stabilized SeNPs. Hence, it can be said that SeNPs are efficient source for photodegradation of organic pollutants.

2.7 ZnS nanoparticles (ZnSNPs)

Zinc Sulfide (ZnS) is an important II-IV direct semiconductor material with a wide band gap i.e., 3.5-3.7 eV for cubic and 3.7-3.8 eV for hexagonal structure and high excition binding energy i.e. 40 meV. This makes it suitable semiconductor material for variety of applications. Concerning the problems of environmental contamination, ZnS has been studied extensively because of their unique catalytic properties to function as a photocatalyst as compared to those of TiO_2. ZnSNPs have been utilized for the photocatalytic degradation of organic pollutants such as p-nitrophenol, p-nitrobenzene, dyes and halogenated benzene derivatives in treatment of wastewater [8]. These studies revealed that ZnSNPs are good photocatalysts because of fast production of electron-hole pairs by photoexcitation and highly negative reduction potentials of excited electrons. ZnS nanospheres displayed good photocatalytic activity for the photodegradation of Eosin B under UV irradiation relative to P25 titania [66]. Further, El-Kemary *et al.* [9] reported the photodegradation characteristics of safranin O dye in the presence of ZnSNPs under UV irradiation. But the efficiency was merely 50%. The

reason can be attributed to the fact that due to short charge separation distances within the semiconductor, recombination of electron-hole pair is too fast resulting in decrease in the quantum yield of the process. Another report showed 63.1% of methyl orange degradation by ZnS after 1 h UV irradiation. Complete degradation of the dye was not observed even after increasing the time of irradiation which may be due to limit of ZnS to generate sufficient free radicals [67].

Therefore, an efficient photocatalyst depends strongly on its efficiency of electron-hole pair separation and its optical absorption properties. Accordingly, the electronic and optical properties of the photocatalyst can be modified so that its photocatalytic efficiency improves.

2.8 Photocatalysis

Photocatalysis, a heterogeneous catalytic system is a combination of photochemistry and catalysis that can be illustrated as a catalytic reaction which is initiated only in the presence of photons of light. In simple words, photocatalysis can be described as the acceleration of the rate of chemical reactions that may be oxidation or reduction in the presence of a catalyst, commonly a semiconductor material by ultraviolet (UV) or visible light irradiation [68]. It is an important stream of chemistry to develop environmental friendly approach for complete degradation and mineralisation of organic pollutants by photocatalytic reaction. A photocatalytic reaction system usually comprises of metal oxides or metal chalcogenide semiconductor characterized by an electronic band structure with valence band and conduction band separated by a bandgap (Eg). Different types of semiconductors were used as photocatalyst, for example, ZnO, TiO_2, ZnS, CdS, CdSe, ZnSe, etc. In this study, we have chosen ZnS semiconductor nanomaterial as a catalyst.

2.8.1 Mechanism of photocatalysis

A schematic representation of the mechanism of photocatalysis is shown in Fig. 3. When the photon of energy higher or equal to the threshold energy, Eg or band gap is absorbed by a semiconductor photocatalyst, holes (h^+_{VB}) and electrons (e^-_{CB}) are generated in valence band (VB) and conduction band (CB), respectively. These charge carriers can either get trapped or they can recombine resulting in dissipating heat energy. Finally, they can react with absorbed species i.e. electron donors or acceptors on the surface of the photocatalyst. Overall photocatalytic efficiency of the photocatalyst is determined by rate of electron-hole pair recombination and electron-hole trapping. The hole will oxidize the adsorbed species, such as

organic compounds, water or hydroxyl ions by the formation of hydroxyl radicals while the electrons react with the compounds present in the solution such as oxygen to form superoxide and hydrogen peroxide to create hydroxyl radicals [69]. The following steps provide a detailed mechanism of photocatalytic degradation of organic compounds by ZnS:

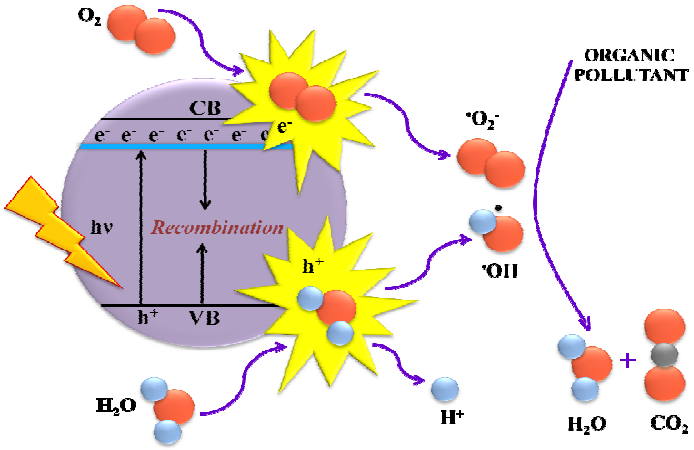

Fig. 3: Schematic mechanism of photocatalysis

Step 1: Photo-excitation of ZnS creating hole (h^+) and free electron (e^-).

$$ZnS + h\nu \longrightarrow e^-_{CB} + h^+_{VB}$$

Step 2: Conversion of surface adsorbed oxygen to form superoxide radical ($^{\bullet}O_2^-$) by e^-_{CB}.

$$e^-_{CB} + O_2 \longrightarrow {}^{\bullet}O_2^-$$

Step 3: Formation of $^{\bullet}OH$ radicals by the reaction of VB hole (h^+_{VB}) with adsorbed H_2O.

$$h^+_{VB} + H_2O \longrightarrow {}^{\bullet}OH + H^+$$

Step 4: Neutralization of superoxide radical ($^{\bullet}O_2^-$) by protonation forming $^{\bullet}HO_2$ radical.

$${}^{\bullet}O_2^- + H^+ \longrightarrow {}^{\bullet}HO_2$$

Step 5: Formation of hydrogen peroxide.

$$e^-_{CB} + {}^{\bullet}HO_2 + H^+ \longrightarrow H_2O_2$$

Step 6: Cleavage of H_2O_2 to form $^{\bullet}OH$ radicals.

$$H_2O_2 + h\nu \longrightarrow 2{}^{\bullet}OH$$

$$h^+_{VB} + OH^- \longrightarrow {}^{\bullet}OH$$

Step 8: Photooxidation of organic compound (R) by $OH^{\cdot}$.

$$^{\bullet}OH + R \longrightarrow CO_2 + H_2O$$

Mostly, these single component semiconductor systems exhibit relatively low photocatalytic efficiency (<5%) since the majority of the photogenerated charge carriers (e^-/h^+) undergo recombination as shown in Fig. 3.

2.9 Co-catalysis

Many semiconductors such as TiO_2, ZnO, and ZnS are being proved as promising photocatalysts for the treatment of organic pollutants due to their strong oxidizing power. However, their comparatively low photocatalytic efficiency due to high recombination rate of photoinduced electron-hole pairs at or near their surface is one of the major drawbacks. This problem can be solved by transporting charge carriers to the surface of the NPs where they will help in suppressing the electron-hole pair recombination rate. Thus, the fabrication of heterostructures plays an important role in photocatalyst's modification.

Studies indicate that the activity of many catalysts can be enhanced when they work in conjunction with some other promoters and these promoters are known as *"co-catalysts"*. Co-catalysts loaded on semiconductors can facilitate oxidation and reduction reactions by providing the active sites/reaction sites while suppressing the electron-hole pair recombination and reverse reactions. It can also provide the trapping sites for the photogenerated electrons and photoinduced holes and promote the charge separation, thus accelerating the photocatalytic process. The co-catalysts catalyze the reaction process by lowering the activation energy and also it could improve the photostability of the catalysts by consuming of photogenerated charges, particularly the holes [70].

Nanomaterial co-catalysts are known to improve the semiconductor catalyst activity by playing a mediating role in storing and shuttling of photogenerated electrons from the semiconductor to an acceptor, acting as a sink for photoinduced charge carriers and hence, promoting interfacial charge-transfer processes. Generally co-catalysts with Fermi level (E_f) lower than semiconductor catalyst are deposited on the semiconductor surface to enhance charge separation. As the Fermi levels of co-catalyst are lower than that of semiconductor, electrons from CB can be easily transferred to co-catalyst NPs, while VB holes remain free

on the semiconductor [10, 70]. This greatly reduces the possibility of electron-hole recombination and resulting in their prolonged separation.

Literature reveals that when semiconductor catalyst and co-catalyst NPs come in contact, the photogenerated electrons are distributed between them. The transference of excited electrons from the semiconductor to co-catalyst continues until the two systems attain equilibration as shown in Fig. 4. The electron accumulation increases the E_f of co-catalyst to more negative potentials and the resultant E_f of the composite system shifts closer to the CB of the semiconductor. The negative shift in the E_f signifies better charge separation and more oxidative/reductive power for the composite system [10]. *Therefore, the coupling of SC catalyst with co-catalyst NPs provides a unique pathway for maximizing the efficacy of photocatalytic reaction system.*

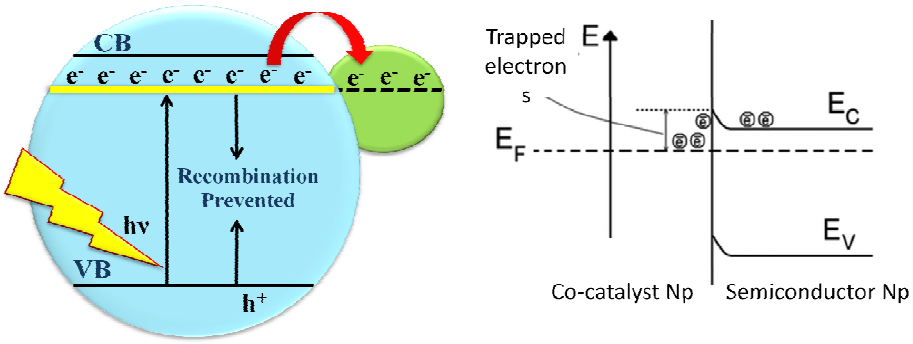

Fig. 4: Effect of co-catalyst on semiconductor and fermi level equilibration in cocatalyst-semiconductor composite

There are several techniques by which co-catalysts can be loaded on semiconductors such as by doping them with metal/non-metal ion, coupling with a narrow band gap semiconductor, nobel metal deposition or forming composite NPs with metal NPs which will help in preventing the recombination of photoexcited electron-hole pairs by improving charge separation and thus, acquiring higher quantum efficiency during photocatalytic reaction [70]. Most of the techniques involved in loading of co-catalyst are physio-chemical. For example, metals like Fe, Cd, Ni, Cu, Zn, Ag, Au, B, etc. were used as co-catalyst for TiO_2 by doping them by different approaches which involve hydrothermal treatment, spray pyrolysis deposition, sol-gel method, magnetron co-sputtering technique, and electrochemical method [11-15]. AgNPs-coated TiO_2 nanofiber composites which showed enhancement in photocatalytic activity for the degradation of organic dyes (such as methyl orange) has been

were prepared by dispersion of TiO_2 nanofibers in silver salt solution under ultrasonication, followed by addition of sodium citrate as a reducing agent [71].

Similarly, many efforts have been exploited to enhance ZnS based photocatalytic activity. Metals ions Mn, Ni, Cu and Fe were doped on ZnS by chemical precipitation for photocatalytic degradation of organic dyes [16, 17]. Se^{4+} doped ZnSNPs were synthesized electrochemically for evaluating its photocatalytic activity on the degradation of indigo carmine dye [18]. *Pal et al.* [72] studied the effect of Au and Pt deposition by solvothermal method on the photocatalytic activity of as-prepared ZnS nanorods which showed improved photooxidation of p-nitrophenol in contrast to bare ZnS and bulk ZnS powders.

Most of the above synthetic methods of doping are characteristic of complex reaction conditions such as the intense ultrasonication, the long aging process, the elevated reaction pressure and temperature, as well as the use of expensive metal salt solutions ($HAuCl_4$, $AgNO_3$, $PdCl_2$, H_2PtCl_6) for seed mediated approach and expensive electrodes (platinum) for electrochemical method. Moreover, these methods are related with various problems including use of harmful chemical agents (hydrazine, surfactants) and production of hazardous commodities. In our study, an effort has been put to improve the photocatalytic activity of ZnS photocatalyst by impregnating biosynthesized SeNPs as co-catalyst on its surface. To the best of our knowledge, this is the first report where biogenically synthesized SeNPs have been used as co-catalyst to improve the catalytic activity of ZnS semiconductor.

2.10 Photocatalytic degradation of dyes

The severity of increasing water pollution has caused alarming situation to take measures for its remediation. Textile industries are one amongst the major industrial sectors causing water pollution due to release of dyes as nearly 80% of the synthetic dyes produced in the world are consumed by them. The discharge of an enormous volume of wastewater containing dyes is an inescapable situation as all dyes used cannot be completely combined with fabric during the dyeing process [73].

Many conventional methods like coagulation, flocculation, precipitation, adsorption, flotation, oxidation, and reduction, electrochemical, aerobic and anaerobic biological treatment are being used for treatment of wastewater. But these methods have fundamental limitations such as incomplete degradation and mineralization of dyes. Simple transfer of hazardous materials from one medium (wastewater) to another (sludge) is not a long-term

solution to the issue of toxic waste loading on the environment [24]. Considering all above factors, much of the present focus is on implementation of heterogenous photocatalysis for complete degradation and mineralization of dyes in industries. This method depends on the formation of highly reactive free radical species that can degrade large number of organic compounds into biodegradable compounds and is known as the advanced oxidation process (AOP) [69].

Degradation of textiles dyes such as indigo carmine, methyl orange, methylene blue, crystal violet, reactive red, sulphur brown and many more by the use of wide range of heterogenous photocatalysts such as TiO_2, ZnO, ZnS, CdS, CdO, CuS, Fe_2O_3 have been reported [24]. Among them TiO_2 and ZnO have been intensively investigated since the discovery of their ability to photocatalyze dyes [74]. Another limitation observed was that upon light irradiation, nanosized ZnO produced a highly active radical species that can quickly oxidize the vat dyes into harmful residues [9].

An approach to enhance the photocatalytic reaction rate can be applied by modifying the semiconductor by loading co-catalyst as discussed already in section 2.8. These series of co-catalyst loaded photocatalysts showed enhanced catalytic activities and selectivities compared to the mono-component photocatalyst. This combined system also provides a more controllable rate of recombination as the composition of two semiconductors with different band gaps can suppress the recombination of e^-/h^+ pairs [16-18, 75-76].

Methyl Orange (MO), Sodium 4-[(4-dimethylamino) phenyldiazenyl] benzenesulfonate is an acid dye (water soluble anionic dye) which is most commonly used for dyeing of fabrics in textile industries and also as a pH indicator. MO is toxic in nature and thus its discharge in water resources will affect the aquatic ecosystem in addition to causing harmful effects such as gastrointestinal irritation with nausea, vomiting and diarrhoea if ingested by humans. It also causes eye and skin irritation upon exposure [MSDS-Methyl Orange]. The sulphonate groups present in this makes it soluble and highly stable causing difficulty in its removal from wastewater.

Many research reports have paid attention to the degradation of acid dyes in the water stream in recent years. However, due to the recalcitrant nature of acid dyes and the high salinity of wastewater containing acid dyes, conventional treatment processes have not proved effective. Adsorption and coagulation methods have also been applied to treat acid dyes in wastewater,

resulting in generation of secondary pollutants [77]. To overcome such limitations, photocatalytic decolorization of water soluble acid dyes can prove effective.

There are limited reports on the photocatalytic degradation of MO by photocatalysts. Among TiO_2 and ZnO photocatalysts, ZnO had showed better photocatalytic activity than TiO_2 but ZnO also showed slow photodegradation of MO [78]. Complex system such as ZnS/TiO_2/Chitosan films [79] and chemically synthesized nanocomposites such as Cr-ZnS [80] have been reported to partially degrade MO. But their complexity and inefficiency to completely degrade and mineralize MO limits their use. However, there is no report on photodegradation of MO by bare ZnS.

Thus, keeping the limitations of various photocatalysts in degradation of MO and the potential use of biogenic co-catalysts in enhancing photocatalytic activity, the aim of our work was to synthesize the Se-ZnS nanocomposites (Se-ZnSNCs) using biogenic Se^0 nanoparticles (SeNPs) as co-catalyst and determine their photocatalytic activity for photodegradation of MO.

3. Materials and Methods

3.1 Materials

Tryptone soya broth (TSB) and tryptone soya agar (TSA) were purchased from Himedia, India. Zinc nitrate [$Zn(NO_3)_2.6H_2O$], L-cysteine [$HSCH_2CH(NH_2)COOH$], ethanolamine (EOA) [$NH_2CH_2CH_2OH$], methyl orange ($C_{14}H_{14}N_3NaO_3S$) were purchased from Loba chemie, India. Sodium selenite (Na_2SeO_3) and absolute ethanol were obtained from Sigma–Aldrich, India. All the chemicals used in the experiments were of laboratory reagent grade and used as received without further purification. Double distilled water was used for preparation of all solutions. The bacterial strain used in the study, *Bacillus sp.*, was earlier isolated from seleniferous soils of Punjab region by our research group.

3.2 Biosynthesis of selenium nanoparticles (SeNPs)

The selected bacterial strain, *Bacillus sp.* was enriched in 250 ml Erlenmeyer flask containing TSB by incubating it at 37°C on a rotary shaker at 120 rpm for 24 h. An inoculum was taken from enriched culture and streaked on TSA plates containing 10mM sodium selenite (SeO_3^{2-}) to confirm the bacterial strain which would produce red colour colonies. The plates were incubated at 37°C for 24-36 h. The red colour colonies were then picked and uniform inoculum was prepared by aseptically transferring a loopful of red colour colony from TSA to 5 ml of sterile TSB in 25 ml test tube and incubated for 24 h at 37°C in an orbital condition. From this 1 ml of active culture was taken and inoculated in 500 ml Erlenmeyer flask supplemented with 10mM Se^{+4}. The culture flask was incubated at 37°C on a rotary shaker at 120 rpm for 48 h. A control flask containing TSB without sodium selenite was inoculated with the same test strain and incubated under the similar conditions.

3.2.1 Recovery of SeNPs from the culture

SeNPs were harvested by separating the bacterial biomass by centrifugation at 2000 rpm for 5-7 min. The supernatant was collected and centrifuged at higher rpm i.e. 12000 rpm for 10 min to collect the NPs. After centrifugation, the upper clear supernatant was discarded and red pellet was washed with distilled water and absolute ethanol 3-4 times and then dried at room temperature to get the isolated SeNPs. The NPs were also preserved in the TSB media at 4°C for future requirements.

3.2.2 Quantification of SeNPs

The concentration of Se in NPs was estimated by acid digestion of the sample. 20 µl of extracted SeNPs were digested with 5ml of 3:1 nitric/perchloric acid and kept in microwave digestor (MARS 6, CHEM) for 1 h. After that 5ml of 6M HCl was added to the digestor tubes and again kept in microwave digestor for 40 min. Thereafter, the digested samples were diluted with distilled water. To determine the concentration of Se present, digested samples were analyzed in fluorescence spectrometer (Perkin Elmer LS-45) after derivatization with 2,3-diamino-naphthalene (DAN). It is based on the reaction of selenites with diamines to produce a piazoselenol which is fluorescent. The excitation wavelength was set at 360 nm.

3.3 Synthesis of zinc sulphide nanoparticles (ZnSNPs)

In a typical synthetic procedure as proposed by Pal *et al.* [25] for ZnSNPs, the solution was prepared by dissolving 0.3 mmol of zinc nitrate and 0.3 mmol of L-cysteine into 100 ml of distilled water. 1 ml of ethanolamine (EOA) was added in it at room temperature, and then the solution was refluxed at 100°C for 24 h in a round bottom flask. The as-synthesized NPs were washed with distilled water 2 times and absolute ethanol 3 times. The NPs were dried in an oven at 80°C and finally ground to fine powder.

3.4 Synthesis of Se impregnated ZnS nanocomposites (Se-ZnSNCs)

Nanoscaled Se impregnated ZnS nanocomposites were synthesized by wet impregnation method followed by calcination. 100 mg of ZnSNPs were mixed with 10 ml distilled water and kept for stirring. To this, 200 µl of 2mg/ml SeNPs solution was added dropwise and the mixture was left for overnight stirring. The product was dried at 80°C and ground to fine powder and finally sintered in muffle furnace at 200°C for 2 h. Various Se-ZnSNCs were prepared by varying the amount of SeNPs (25-200 µl). The percentage weight of SeNPs in ZnS in each sample was also calculated.

3.5 Characterization techniques

3.5.1 UV-Visible Spectroscopy

UV-Visible spectroscopy was used to characterize NPs because the absorption spectra gives preliminary data on the NP shape and size distribution as NPs have optical properties that are sensitive to size, shape, concentration, agglomeration state, and refractive index near the NP

surface, which makes UV-Vis spectroscopy a valuable tool for identifying, characterizing, and studying these materials. Analysis has been done on a double beam **Spectrophotometer (Analytikjena Specord 205)** by taking ≈ 2.5 ml NP solution in a 3.5 ml quartz cuvette within the range of 190−1100 nm and setting the baseline with water. The band gap (Eg) of as-synthesized photocatalyst was calculated using the equation:

$$Eg\ (\text{eV}) = 1240/\lambda$$

where, Eg is band gap energy (in electron volts), and λ is the wavelength (nm) at the absorbance maxima. Further, optical band gap was determined by using Tauc Equation:

$$\alpha h\nu = A(h\nu - Eg)^n$$

where α is the absorption coefficient of the material, which represents the absorption ability of a material for a certain wavelength; h is the Planck constant; ν is the frequency of light; A is a constant, which depends on temperature, photo energy and phonon energy; Eg is the band gap; the exponent n is a characteristic of the type of electrons transition process (n = 1/2 for a direct allowed transition & n = 2 for an indirect allowed transition process). As ZnS is direct band semiconductor, the value of n taken is 1/2 [81].

Photodegradation study of the compound was also determined via spectroscopic analysis by scanning the resultant degraded solution in the range of 200-800 nm.

3.5.2 Dynamic Light Scattering (DLS)

This technique is most commonly used to analyze the size of the NPs. The particles suspended within a liquid undergo Brownian motion. The larger the particle, the slower the Brownian motion will be. The Brownian motion of particles or molecules in suspension causes laser light to be scattered at different intensities which is monitored by DLS. Analysis of these intensity fluctuations yields the velocity of the Brownian motion and hence the particle size by using the Stokes-Einstein relationship:

$$D = k_B\, T/6\, \pi\, \eta\, r$$

where k_B is Boltzmann's constant, T is absolute temperature, η is viscosity and r is the radius of the spherical radius. The analysis was done by taking ≈ 1.5 ml of the dispersed particles in a cuvette by means of **DLS system (Brookhaven 7610).**

3.5.3 X-Ray Diffraction (XRD) Analysis

Structural and phase identification of the composites was carried out on **X-ray Diffractometer (PANalytica X'pert PRO).** X-ray diffraction is based on constructive interference of monochromatic X-rays and a crystalline sample. X-rays are produced by bombarding a metal target (Cu, Mo usually) with a beam of electrons emitted from a hot filament (often tungsten) from a cathode ray tube. These rays are filtered by crystal monochrometers to produce monochromatic X-rays needed for diffraction. They are then aligned and directed onto the sample. When the geometry of the incident X-rays striking the sample satisfies the Bragg Law, constructive interference occurs and a peak in intensity occurs. Bragg's Law gives the conditions for constructive interference according to the following equation:

$$n\lambda = 2d \sin\theta$$

These diffracted X-rays are then detected by detector and processed by a computer monitor. The samples are scanned by X-ray detector through a range of 2θ angles so that all possible diffraction directions of the lattice are attained due to the random orientation of the powdered material. The analysis was done by using Cu-Kα (k = 1.54060 A°) radiation operated at 45 kV in the range of 2θ = 10-80° with 0.013 step size and a counting time of 29 secs per step. The composites to be analyzed were prepared by grinding dried powder in a pestle and mortar to form fine and homogenised powder. Also, the crystallite size of NPs was calculated from the Scherrer's equation:

$$d = \frac{0.9\,\lambda}{\beta\, cos\theta}$$

where λ is x-ray wavelength, β is the full width at half maximum (FWHM) of the diffraction peaks and θ is the diffraction angle.

3.5.4 Scanning Electron Microscopy (SEM)

SEM was used to obtain information about the surface morphology of the sample. SEM images provide information in terms of topography, external morphology (size, shape and arrangement), composition, and crystalline structure and orientation of the sample surface. Data are generated by selecting area of the surface of the sample to be analyzed, and a 2-dimensional image is generated that shows the spatial variations in these properties. **SEM**

(JSM-7600F (0.1–30 KV)) was used for surface morphology analysis of sample. Samples were prepared by mixing 1mg of powdered sample in ethanol through sonication for 1 h. After that the solution was treated with an ultrathin coating of electrically conducting Au material, which was lodged on the sample by low-vacuum sputter coating. After that, conducting material was mounted rigidly on a specimen holder called a specimen stub and the samples were visualized under SEM for surface analysis.

3.5.5 Energy Dispersive X-ray (EDX) Spectroscopy

EDX is an analytical tool used for identification or mapping of elements present in the composites. EDX detector separates the characteristic x-rays of different elements into an energy spectrum, and EDX system software analyzes the energy spectrum in order to determine the abundance of specific elements. It can provide elemental analysis on areas as small as nanometers in diameter as well as can create element composition maps over a much broader selected frame. This technique was used to study the chemical composition of the selected points or areas of the sample. It was also helpful in identifying materials and contaminants and even in distinguishing their relative concentrations on the surface of the sample. EDX analysis was carried on **JSM-7600F.**

3.5.6 Surface Area Analysis

Brunauer, Emmett and Teller (BET) surface area analysis was carried out in order to measure the surface area of the powdered samples. The principle of BET analysis is physical adsorption of a gas on the surface of the solid sample. The amount of gas adsorbed corresponding to a monomolecular layer on the surface is measured by a volumetric or continuous flow procedure. The analysis of the porous surface was carried out by N2 adsorption/desorption techniques at 77°C. Adsorption isotherms were determined using a **BET surface area instrument (Smartsorb 92/93)** where 100 mg of samples are regenerated at 150℃ for 1 h.

3.5.7 Gas Chromatography

The amount of CO_2 evolved from the photocatalytic degradation was determined by using gas chromatography **(NUCON-5765)** with **Propak-Q column**. It involves a sample being vapourised when injected onto the head of the chromatographic column. The sample is transported through the column by the flow of mobile phase which comprises of inert gases like nitrogen, helium or argon. The stationary phase contains a column where the packing or

solid support itself acts as stationary phase, or is coated with the liquid stationary phase like high boiling polymer which is adsorbed onto the surface of an inert solid. The detector i.e. thermal conductivity detector (TCD) senses the difference in thermal conductivity of two gases flows i.e. the inert carrier gas and the sample. Changes in the temperature of the electrically-heated wires in the detector are affected by the thermal conductivity of the gas which flows around this. So, the changes in this thermal conductivity are sensed as a change in electrical resistance and are monitored.

The CO_2 evolution was determined by injecting 1 ml of the gaseous mixture from the reaction tube into the gas chromatography using Propak-Q column (30 mm × 0.32 mm × 12.00 μm) with nitrogen as carrier gas (30 ml/min) and thermal conductivity detector (TCD). Column oven was maintained at 40°C while injector and detector were at 70 and 80°C, respectively.

3.6 Photocatalytic reaction setup

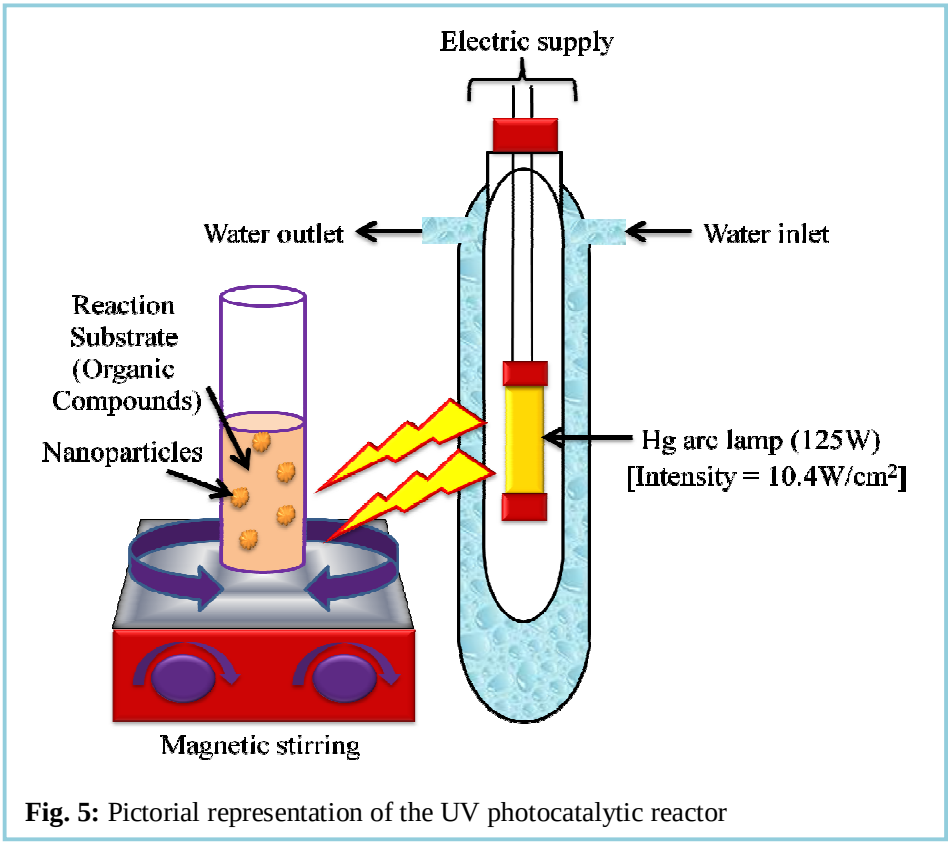

Fig. 5: Pictorial representation of the UV photocatalytic reactor

Fig. 5 represents the photocatalytic reactor. It is composed of a UV light source (125 W) of low pressure mercury vapour lamp that emits mainly at 254 nm. The Hg lamp (125 W; intensity 10.4 mW/cm^2) connected to power cords is set inside a water-jacketed quartz tube. A continuous flow of cold water is circulating in the outer jacket to make sure that it remains

cool for a longer time and to avoid overheating of the lamp. A maximum amount of 5 ml reaction sample is taken in 15 ml capacity test tube that is placed at a distance of 4-5 cm from light source under continuous magnetic stirring. The distance between magnetic stirrer and lamp is minimized to get optimum flux. The whole set up is placed in a wooden box to prevent direct UV exposure as a safety purpose. The photocatalytic reaction was carried out to check the activity of synthesized NPs for degradation of organic pollutants in the presence of UV irradiation.

3.7 Dye degradation

The batches of 40 µM methyl orange (MO) dye solution was treated with 20 mg of Se NPs, ZnSNPs and Se-ZnSNCs to study the comparative degradation efficiencies of the NPs. The NPs were weighed and mixed with the MO dye solution by sonicating for 5-10 min. The photocatalytic degradation was initiated by continuous stirring of the test tubes containing dye treated with NPs in the presence of the UV lamp. The kinetics of decolorization of the dye was studied by withdrawing sample test tube after every 20 min and centrifuging at 12,000 rpm at 25°C for 5 min. The same was repeated till the MO dye became colorless. The absorbance of the supernatant MO dye solution was measured by scanning the sample in UV-Vis spectrophotometer. The λ_{max} of MO was 460 nm.

4. Results and Discussion

4.1 Biosynthesis of Se nanoparticles (SeNPs)

Selected bacterial strain, *Bacillus sp.* was cultivated in TSA and active culture was taken for the synthesis of Se^0. Red Se^0 synthesized after exposing the strain to 10mM sodium selenite and incubating for 48 h in the TSB media at 37°C. The bacteria caused the reduction of SeO_3^{2-} to Se^0 as detected by the formation of red colored precipitates in the media. When the activated bacterial strain was inoculated in TSB without sodium selenite, the other reaction conditions remaining the same, the color of the reaction broth did not change, indicating that no Se^0 was synthesized by bacteria in the absence of sodium selenite. Thus, the bacterial isolate reduced the selenite ions (SeO_3^{2-}) aerobically conjoined with formation of SeNPs in the culture medium.

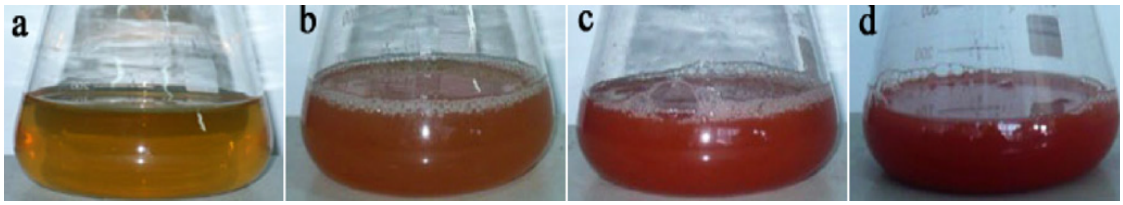

Fig. 6: The time-dependent color changes of the reaction broth in the synthesis of SeNPs; **(a)**, **(b)**, **(c)** and **(d)** represent 0, 12, 24 and 48 h of incubation, respectively

Fig. 6 displays change in the color of the TSB media with time indicating the formation of SeNPs. At the beginning, the media was yellow in color which started becoming red after 10-12 h of incubation and the intensity of red color kept on increasing with time. After 48 h of incubation there was no color change observed further indicating the complete reduction of SeO_3^{2-} to elemental Se^0. The characteristic red color of the reaction solution was due to excitation of the surface plasmon vibrations of the α-Se particles in form of nanospheres providing a convenient spectroscopic signature of their formation [82]. The size of the SeNPs showed direct relationship with the time of incubation with increase in size over increasing incubation time. Tam *et al.* [83] reported similar representative results in the generation of Se^0 NPs by *Shewanella* sp HN-41 showing an increase of size and amount of NPs with time. The amount of Se present in the as-synthesized NPs were estimated to be 2mg/ml which represents that appropriate amount of Se^0 is being produced by bacteria by reduction of SeO_3^{2-}.

4.1.1 Optical characterization and DLS studies of SeNPs

Further characterizations of the as-synthesized SeNPs were carried out to determine its properties i.e. size and shape. The UV-Visible spectroscopy was done by scanning the SeNPs recovered from the reaction broth after washing between the ranges of 200-1100 nm. The UV-Visible absorption peak was observed depending on the size of the NPs. The characteristic peak was observed at 620 nm (Fig. 7) which corresponds to particle size of 101.6 ± 9.8 nm [84]. The size of the SeNPs was further confirmed by DLS data which indicated the size distribution pattern of SeNPs ranging from 50-200 nm with an average hydrodynamic diameter of 91 nm as shown in Fig. 8.

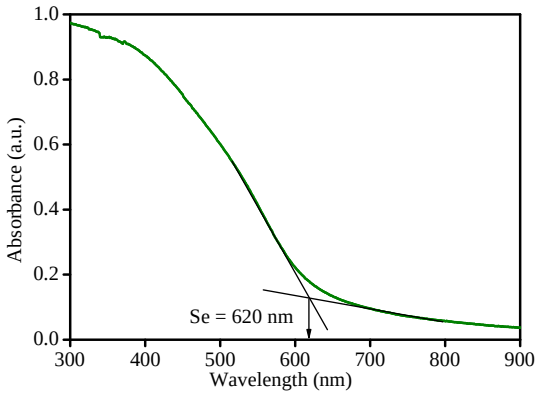

Fig. 7: Absorption spectra of SeNPs

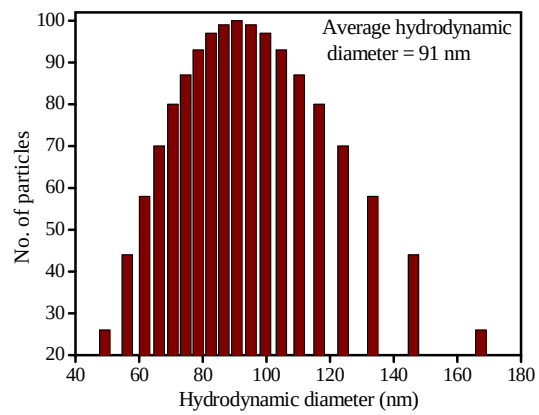

Fig. 8: Particle size distribution of SeNPs

4.1.2 XRD analysis of SeNPs

X-ray diffraction analysis was performed to characterize the composition and structure of the resultant samples. The curve in Fig. 9 depicts a typical X-ray diffraction pattern of SeNPs. We assumed that precipitation of Se was amorphous in nature, which was in agreement with the results of XRD curve as reported by Kaur *et al.* [85]. The XRD pattern of the SeNPs showed no clearly sharp Braggs reflections except for a broad peak at the 2θ angles 15° to 35°, confirming that the SeNPs are not in a crystalline phase i.e. the polymorph of the obtained SeNPs is amorphous Se. The XRD pattern matched very well with that of the standard literature value (JCPDS File No. 073-2699) of selenium powder confirming the formation of SeNPs.

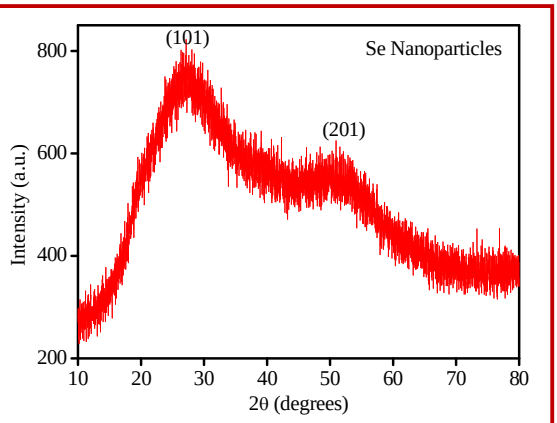

Fig. 9: Powder XRD pattern of SeNPs

4.1.3 SEM-EDX analysis of SeNPs

The morphological and dimensional study of SeNPs collected from the reaction media was done by scanning electron microscopy (SEM). SEM was performed to determine the shape and size of the particles. SEM images (Fig. 10(a-d)) showed that the SeNPs are produced extracellularly by the bacteria and had a spherical morphology with smooth surface. There were numerous particles and size of the NPs was in broad range of 50-200 nm. Also, the EDX spectrum was taken to investigate composition of the SeNPs which proved that they were composed of selenium (Fig. 10e). The presence of carbon and oxygen is presumed to be due to the presence of biomass from where SeNPs have been recovered.

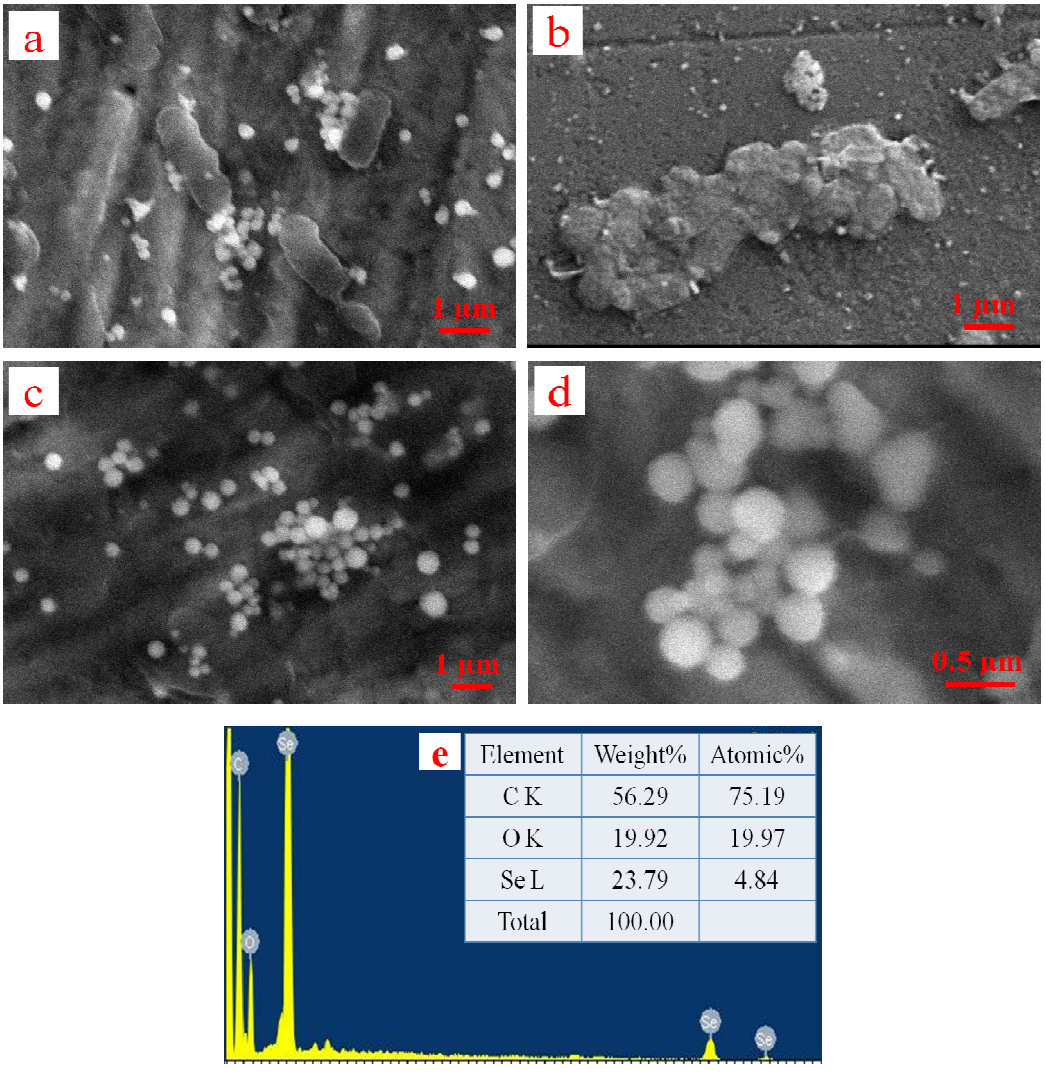

Element	Weight%	Atomic%
C K	56.29	75.19
O K	19.92	19.97
Se L	23.79	4.84
Total	100.00	

Fig. 10: SEM images of SeNPs produced by *Bacillus sp.* in TSB Media; **(a-b)** Cells grown in TSB plus 10mM sodium selenite, **(c-d)** Spherical SeNPs produced by bacterial cells and **(e)** EDX profile of SeNPs

4.2 Synthesis of ZnS nanoparticles (ZnSNPs)

ZnSNPs were synthesized by the method as reported by Pal *et al.* [25] where L-cysteine was used as a source of sulfur. ZnSNPs formed at 100°C with a cubic structure as determined by the XRD analysis of the resultant sample. Fig. 11 represents the scheme for the formation of ZnSNPs. In this reaction, as $Zn(NO_3)_2.6H_2O$ was dissolved in water, Zn^{2+} ions could form a variety of complexes in the solution, and then this was hydrolyzed to form $Zn(OH)_2$. During the reaction process, $_L$-cysteine would release sulphide ions that would react with zinc ions. As a result, ZnSNPs form via an in situ chemical reaction. The possible general chemical reactions for the synthesis of ZnSNPs are as follows:

$$Zn(NO_3)_2.6H_2O \longleftrightarrow Zn(OH)_2 + 2HNO_3$$

$$HSCH_2CH(NH_2)COOH \longleftrightarrow CH_3COOH + H_2S + NH^+$$

$$H_2S \longleftrightarrow HS^- + H^+,\ HS^- \longleftrightarrow S^{2-} + H^+$$

$$Zn^{2+} + S^{2-} \longrightarrow ZnS$$

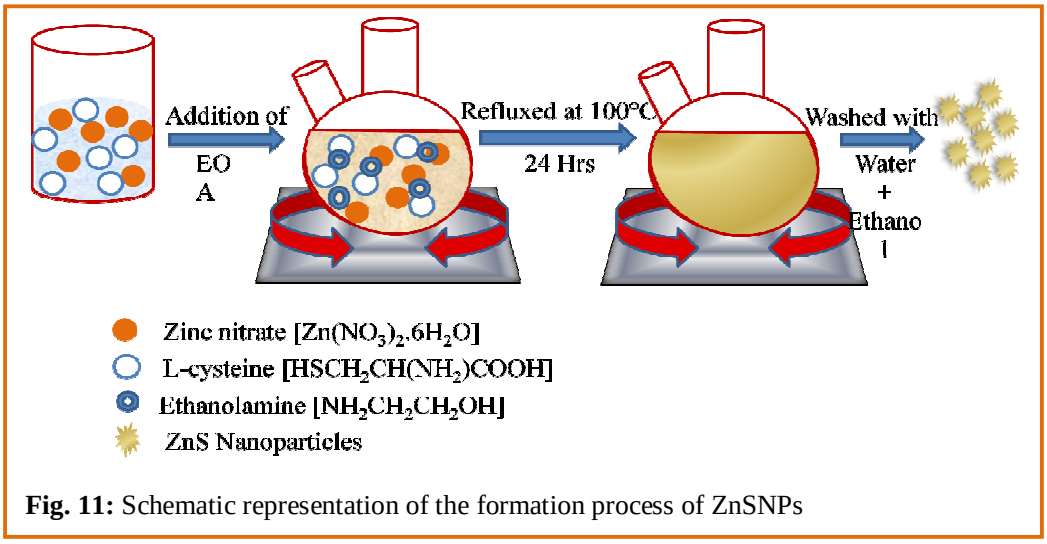

Fig. 11: Schematic representation of the formation process of ZnSNPs

4.2.1 Optical characterization of ZnSNPs

In order to study optical absorption property of the samples, the ZnSNPs were ultrasonically dispersed in double distilled water and the UV-Vis absorption spectrums of the prepared samples were taken and compared with absorption spectrum of bulk ZnS as shown in Fig. 12. From the curve, the shoulder was observed near 330 nm in the spectrum for the pure ZnSNPs and around 400 nm for bulk ZnS. Therefore, the absorption peak of ZnSNPs considerably blue-shifted compared to that of bulk ZnS. This absorption shift is due to quantum size effect,

representing a change in band gap and resulting in a more discrete energy spectrum of NPs formed. The shoulder or peak of the spectra corresponds to the fundamental absorption edges in the samples, which will be used later to estimate the band gap of the materials synthesized.

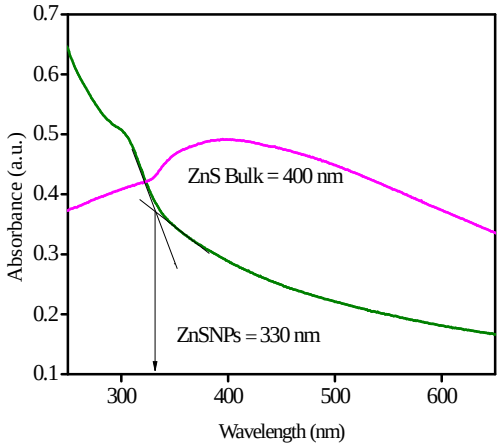

Fig. 12: Absorption spectra of ZnSNPs

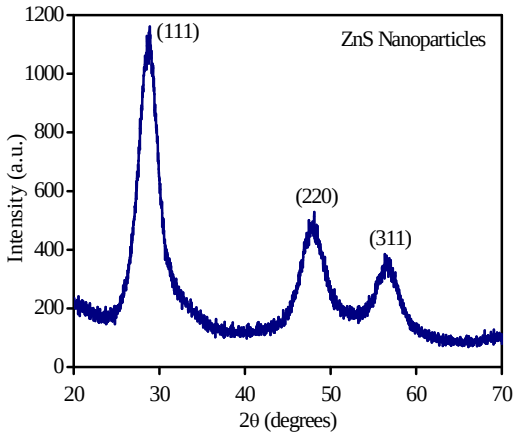

Fig. 13: Powder XRD pattern of ZnSNPs

4.2.2 XRD analysis of ZnSNPs

The powder X-ray diffraction (XRD) pattern of ZnSNPs is shown above in Fig. 13. The spectra shows three diffraction peaks at 2θ values of 28.82°, 48.04° and 56.56° corresponding to the diffraction planes (111), (220) and (311), respectively. These peaks were perfectly indexed to the cubic phase of ZnS. All the peaks identified were close to the reported value for cubic ZnS (JCPDS File No. 79-0043). The crystallite size was calculated by using Scherrer's equation which was around 4 nm. No other crystalline impurities were detected by XRD, indicating that pure wurtzite ZnS can be obtained via the mild reaction conditions.

4.2.3 SEM-EDX analysis of ZnSNPs

Fig. 14 shows the morphological and compositional characterization of as-synthesized ZnSNPs carried out by SEM-EDX. The Fig. 14 (a-b) clearly demonstrate that ZnSNPs produced are spherical in shape with rough surface which also resemble sponge and porous like structures. The average size of ZnSNPs can be estimated to be 100-150 nm. The EDX spectrum in Fig. 14(c) showed the elemental composition of ZnSNPs in which Zn and S are in 70:30 ratios.

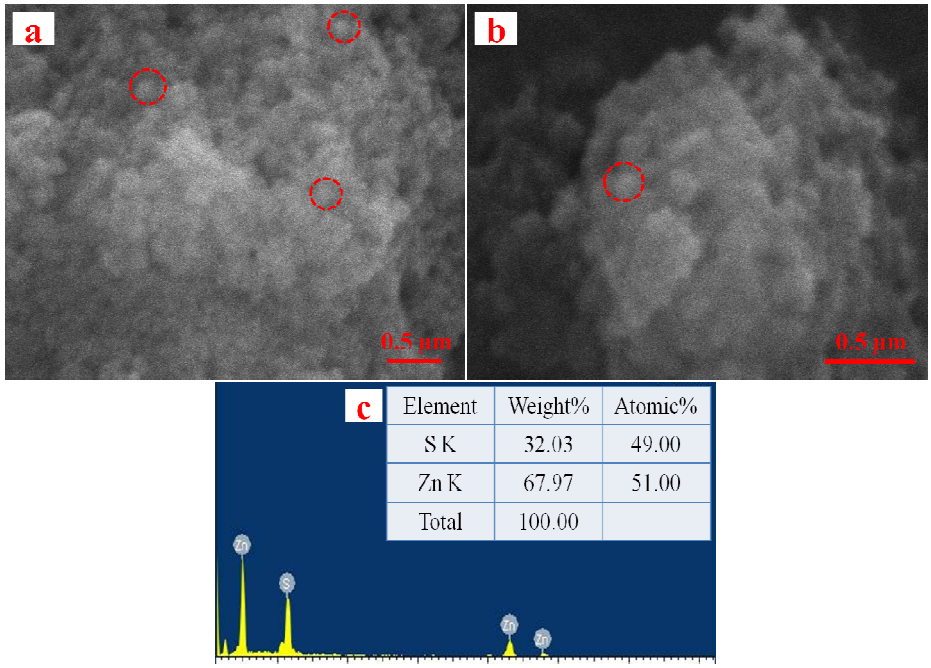

Figure 14: (a-b) SEM images of ZnSNPs and **(c)** EDX profile of ZnSNPs

4.3 Synthesis of Se impregnated ZnS nanocomposites (Se-ZnSNCs)

Se-ZnSNCs were prepared by wet impregnation method followed by calcination. Wet impregnation is a well known procedure for the development of heterogeneous catalysts. Moreover the use of this method without any additional treatment before the subsequent heating in a controlled atmosphere is an easy procedure for obtaining nanocomposites. The general scheme for the formation of Se-ZnSNCs is represented in Fig. 15.

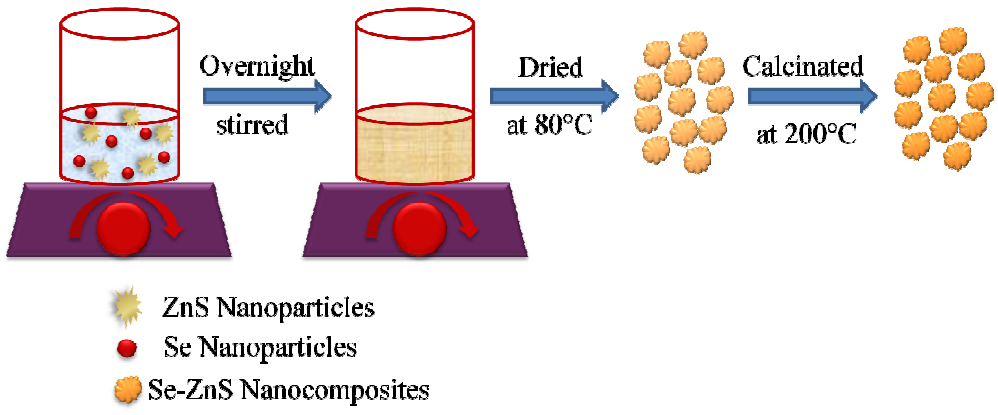

Fig. 15: Schematic representation of the formation process of Se-ZnSNCs

The percentage weight of Se present in various Se-ZnSNCs (25 to 200 µl) was calculated as shown in the following Table 2.

Table 2: Calculation for Se wt%

Amount of SeNPs	Conc. of Se	Se wt% with respect to 20 mg ZnS
25 µl	0.05 mg	0.25%
50 µl	0.1 mg	0.5%
100 µl	0.2 mg	1%
200 µl	0.4 mg	2%
1 ml SeNPs solution = 2 mg Se		

4.3.1 Optical characterization of Se-ZnSNCs

The UV-visible absorption spectrum of Se-ZnSNCs is being represented in Fig. 16 in comparison to that of bare Se and ZnS NPs. The absorption shoulder appeared at 357 nm. The red shift has been observed as compared to UV-Visible spectrum of ZnSNPs (330 nm). The red shift in the absorption shoulder for Se-ZnSNCs is related to the band gap decrease of ZnS when Se is impregnated onto ZnS. From this shift it can be interpreted that SeNPs which shows absorption in visible region i.e. 620 nm has been deposited on ZnSNPs. The visible color change in as-synthesized nanocomposites was also indicative as shown in the inset of Fig. 16.

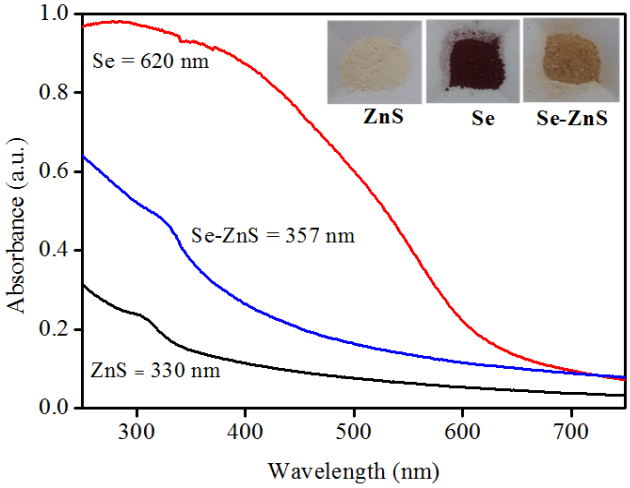

Fig. 16: UV-visible absorption spectra of bare Se, ZnS and 1wt% Se loaded ZnSNCs

The band gap of as-synthesized photocatalyst was calculated using the equation:

$$Eg\ (\text{eV}) = 1240/\lambda$$

where, *Eg* is band gap energy (in electron volts), and λ is the wavelength (nm) at the absorbance maxima. The band gap energy for pure ZnSNPs and Se-ZnSNCs were 3.77 and

3.47 eV, respectively. It is evident that the Se-ZnSNCs should be photocatalytically active in the UV light. These calculated band gap values are in agreement with the values calculated by tuac's plot as shown in Fig. 17.

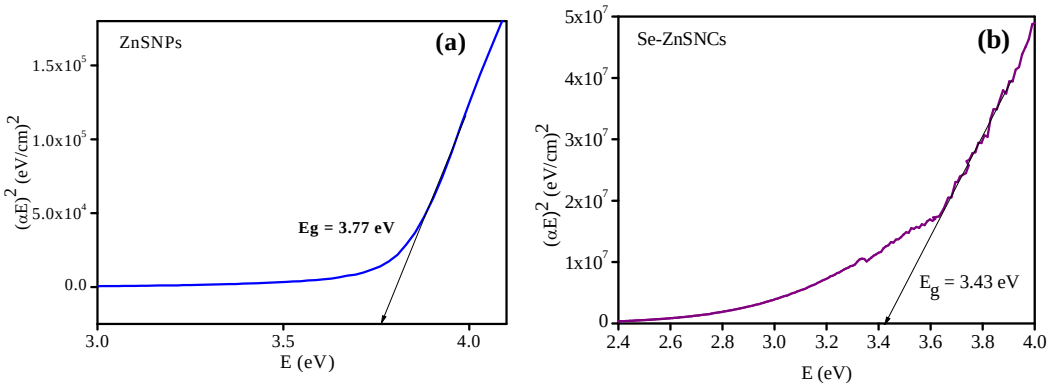

Fig. 17: Band gap of **(a)** bare ZnSNPs and **(b)** 1wt% Se loaded ZnSNCs

4.3.2 XRD analysis of Se-ZnSNCs

The structural analysis of the synthesized Se-ZnSNCs in comparison to pure ZnSNPs has been carried out by XRD measurements as shown in Fig. 18. Fig. 18(a) shows the XRD spectra of ZnSNPs as described in Fig. 17 above. The XRD pattern of the Se-ZnSNCs in Fig. 18(b, c) shows total six diffraction peaks with 2θ values of 27.36°, 28.82°, 30.84°, 48.04°, 52.43° and 56.56° corresponding to the diffraction planes (100), (111), (101), (220), (201) and (311), respectively. The diffraction peaks with planes (100), (101) and (201) match the 2θ angles listed for a hexagonal selenium phase in JCPDS File No. 006-0362 [86] and the rest are of cubic phased ZnSNPs. The diffraction peaks corresponding to Se directly indicate its presence and thus the formation of Se-ZnSNCs which is further confirmed by the EDX of these NCs.

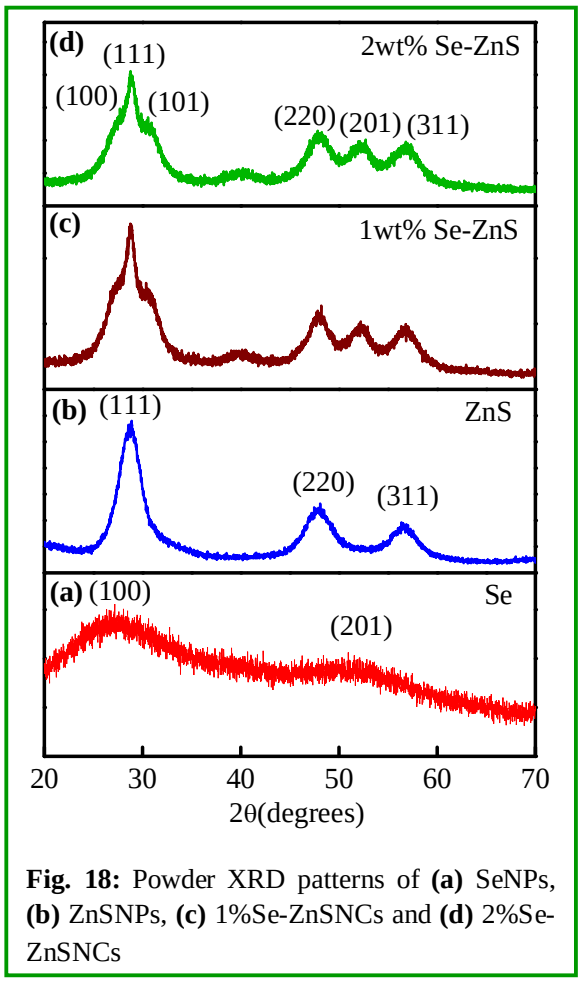

Fig. 18: Powder XRD patterns of **(a)** SeNPs, **(b)** ZnSNPs, **(c)** 1%Se-ZnSNCs and **(d)** 2%Se-ZnSNCs

4.3.3 EDX analysis of Se-ZnSNCs

The elemental analysis of Se-ZnSNCs were carried out using EDX (Fig. 19) which confirms the presence of 0.17, 0.26, 0.36 and 0.43 weight % of Se in 0.25wt%, 0.5wt%, 1wt% and 2wt% impregnated Se-ZnS samples respectively.

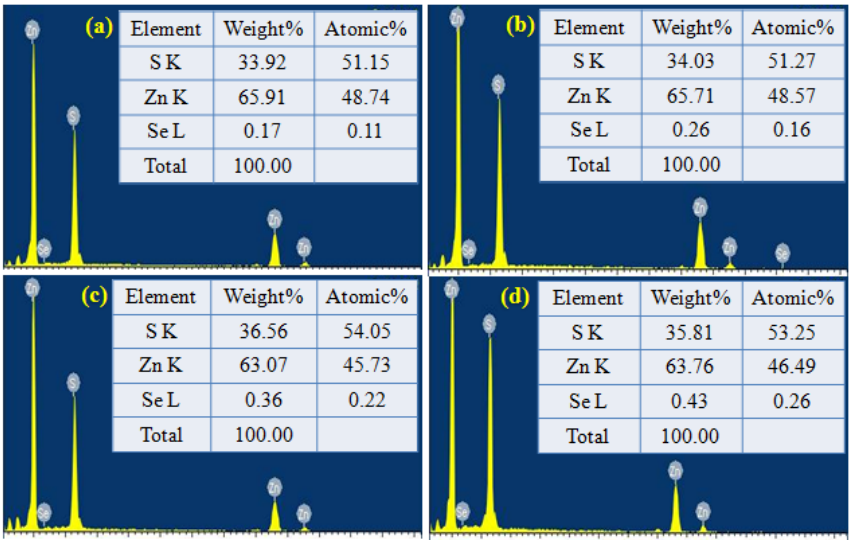

Fig. 19: EDX profiles of **(a)** 0.25wt% Se-ZnS, **(b)** 0.5wt% Se-ZnS, **(c)** 1wt% Se-ZnS, and **(d)** 2wt% Se-ZnS

4.3.4 BET analysis

The BET surface area (S_{BET}) of 0.25wt% Se-ZnSNCs, 0.5wt% Se-ZnSNCs, 1wt% Se-ZnSNCs and 2wt% Se-ZnSNCs was found to be 67.2 m^2/gm, 69.5 m^2/gm, 74.6 m^2/gm and 75.3 m^2/gm, respectively. All the respective BET surface areas were more than the surface area of the bare ZnSNPs i.e. 54.4 m^2/gm. This increase in the surface area of the NCs may be due to the deposition of SeNPs on the surface of the ZnSNPs. Alteration in surface area of NCs relative to bare ZnS signifies the presence of SeNPs on ZnS.

4.4 Photocatalytic activity

To evaluate the photocatalytic activity of as-synthesized SeNPs, ZnSNPs and Se-ZnSNCs, studies of photocatalytic degradation experiment was carried out by choosing methyl orange (MO) dye as a model test substance. The dye concentration of 40 µM was taken. The progress of the dye decolorization was monitored by the decrease in absorbance of the maximum peak value at 460 nm.

4.4.1 Control experiments

The decolorization of the 40 µM MO dye solution was followed initially using control experiments. Dark absorption was studied to understand the effect of light towards degradation of dye by keeping the MO dye solution for 1 h under constant stirring with catalyst in dark chamber. The concentration of MO with the addition of Se-ZnSNCs and Se was stable in 1 h. In case of ZnS, the MO concentration decreased by 18% as shown in Fig. 20(a). Similarly, to analyse the effect of photolysis on MO dye solution, it was irradiated under UV light for 2 h under constant stirring. No degradation [Fig. 20(b)] was evident in this condition indicating that MO has a good photostability under the UV light irradiation as reported in the literature [87].

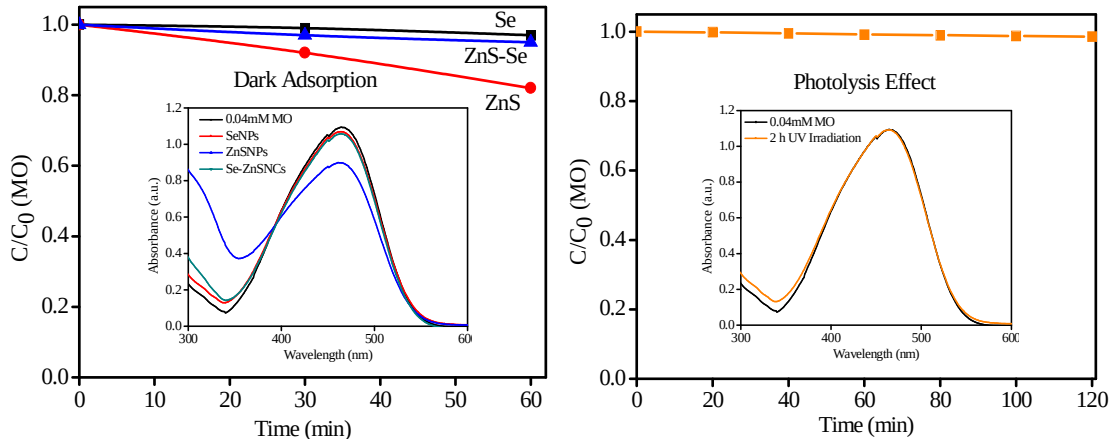

Fig. 20: (a) 1 hr dark adsorption study by Se, ZnS and Se-ZnS photocatalysts and **(b)** Photolysis study of MO under 2 hr UV irradiation

4.4.2 Effect of SeNPs, ZnSNPs and Se-ZnSNCs on photocatalysis

Fig. 21 illustrates comparative study of photodegradation efficiency by SeNPs, ZnSNPs and Se-ZnSNCs in 1 h duration. About 8.45%, 23.02% and 48.72% decolorization of MO (40 µM) was observed after 1 h UV irradiation with the photocatalyts Se, ZnS and Se-ZnS respectively. The low catalytic activity of SeNPs may be attributed to their amorphous nature which makes it unstable to carry out the electron/hole recombination process for photodegradation which is in agreement with literature [65] wherein only TX-100 stabilized SeNPs showed photodegradation. Although the SeNPs showed absorption peak in visible region, photocatalyic activity carried out in visible did not show any degradation of the dye. The degradation efficiency of the ZnS and Se-ZnS photocatalysts was in good agreement with the surface properties of the photocatalysts as analysed by the BET surface area

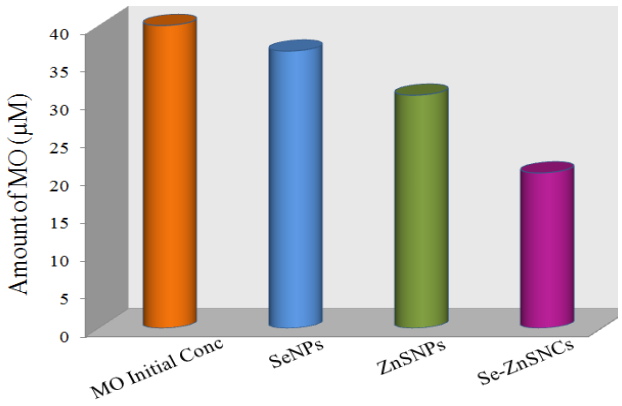

Fig. 21: Comparative study of photodegradation of MO by SeNPs, ZnSNPs and Se-ZnSNCs under 1h UV irradiation

analysis. Se-ZnSNCs had higher surface area between 67-75 m^2/gm as compared to surface area of ZnSNPs which was 54.4 m^2/gm. In addition, higher photocatalytic degradation of dye using Se-ZnS compared to pure ZnS may be due to trapping of photo-excited electrons at conduction band by the SeNPs, thereby decreasing the electron-hole recombination.

4.4.3 Effect of variable Se concentration (wt%) on photocatalytic degradation by Se-ZnSNCs

The co-catalytic efficiency of SeNPs has been comparatively studied for the UV induced photooxidation of MO (0.04mM) by carrying out experiment with 0.02 g of each ZnSNPs and 0.25wt%, 0.5wt%, 1wt% and 2wt% Se-ZnSNCs. Test tubes containing 5 ml of 40 µM MO dye solution were stirred for 1h in dark to achieve adsorption equilibrium and were then irradiated with UV light. After every 20 min samples were collected and absorbance was taken of the supernatant dye solution till it became colorless. Fig. 22 depicts the photodegradation trend followed by ZnSNPs and 0.25wt%, 0.5wt%, 1wt% and 2wt% Se-ZnSNCs under 160 min of UV irradiation.

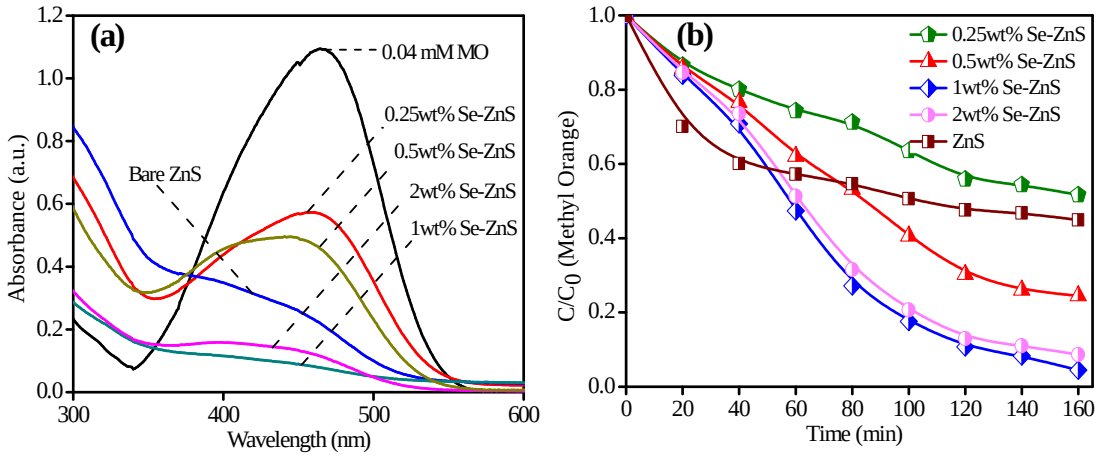

Fig. 22: (a) Changes in the absorption spectra of MO (λmax = 460 nm) under 160 min UV irradiation and **(b)** time course of photodegradation of MO (0.04mM) by ZnSNPs and 0.25wt%, 0.5wt%, 1wt% and 2wt% Se-ZnSNCs under UV irradiation

Fig. 22(a) shows the changes in the absorption intensity of MO (0.04 mM) during its photooxidation by addition of respective photocataylst under 160 min UV light irradiation. The absorption intensity (1.09 a.u) of 0.04 mM MO decreases in a varied extent by bare ZnS and different Se-ZnS photocatalysts. The 1wt% Se-ZnSNCs degrade MO (abs. 0.095 a.u.) appreciably as compared to bare ZnS (abs. 0.27 a.u.). This difference in the photooxidation efficiency of MO by Se-ZnSNCs could be ascribed to the additional energy levels of the impregnated Se that store a fraction of electrons captured from photoexcited semiconductor [70] and hence, improves the photocatalytic efficiency. In a similar way, the time course of photocatalytic degradation of 5 ml (0.04 mM) MO by ZnSNPs and 0.25wt%, 0.5wt%, 1wt% and 2wt% Se-ZnSNCs has been displayed in Fig. 22(b). It depicts the extent of degradation (C/C_0) from initial MO concentration of 0.04 mM versus irradiation time (T) in which C is the absorbance of substrate solution at each time interval of irradiation and C_0 is the absorbance of the initial concentration.

The total percentage of 0.04 mM MO photodegraded by ZnSNPs and 0.25wt%, 0.5wt%, 1wt% and 2wt% Se-ZnSNCs is displayed in Fig. 23. Se-ZnS photocatalyts showed higher activity as compared to ZnS (55.09%) which is also due to the adsorption (Fig. 25a). Among Se-ZnSNCs, 1wt% Se-ZnS showed maximum degradation of 95.51% in 160 min.

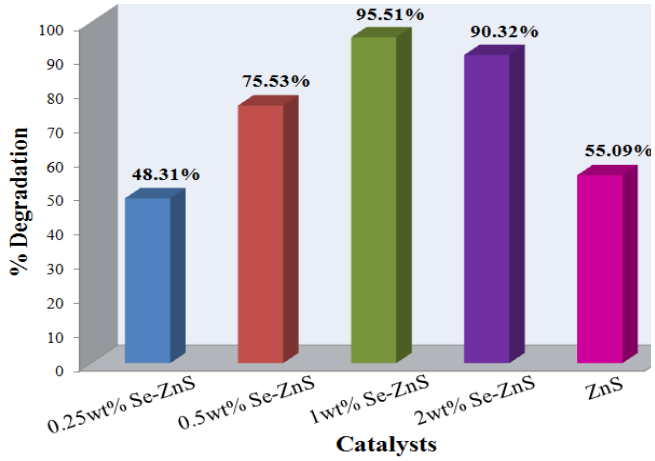

Fig. 23: Effect of variable Se concentration (wt%) on ZnSNPs for photocatalytic degradation of MO

The photocatalytic activity of catalyst is enhanced due to the energy levels of the impregnated material. When surface of ZnS is exposed to UV irradiation, electron-hole pairs are generated. Holes are generated in valence band and excited electrons move towards the covalent band. The excited electrons are highly unstable and can revert back to valence band in fraction of seconds failing the recombination of electron-hole pair resulting in the absence of the generation of hydroxyl radicals and superoxide ions necessary to carry out degradation. On contrast, in case of Se-ZnS photocatalyst, the high photocatalytic activity is due to the additional energy levels of the impregnated Se. The excited electrons are trapped by the

conduction band when the energy levels of the deposited NP lie below it. Similarly, when the energy level is above the valence band, electrons can quench the photogenerated holes [88]. It can be hypothesized that with its energy level (2 eV), Se may act either as an electron or a hole trap which enhances the separation of the electron-hole pairs in the semiconductor. When it traps the electron, its electronic configuration is disturbed. The trapped electron gets readily transferred to oxygen molecule to produce superoxide radical ion. Se can also trap the hole to retain its stable electronic configuration. Alternatively, when Se traps the hole its electronic configuration is disturbed. The trapped hole gets readily transferred to hydroxyl ion adsorbed on the surface of ZnS to produce hydroxyl radical.

Hence, when Se is impregnated on ZnS, more trap sites for electrons and holes are generated, more electron-hole pairs are produced and thus causing an increase in the amount hydroxyl radicals and superoxide ions responsible for the degradation of organic pollutant. As a result, the photocatalytic activity of ZnS is increased.

4.4.4 Photocatalytic degradation of methyl orange

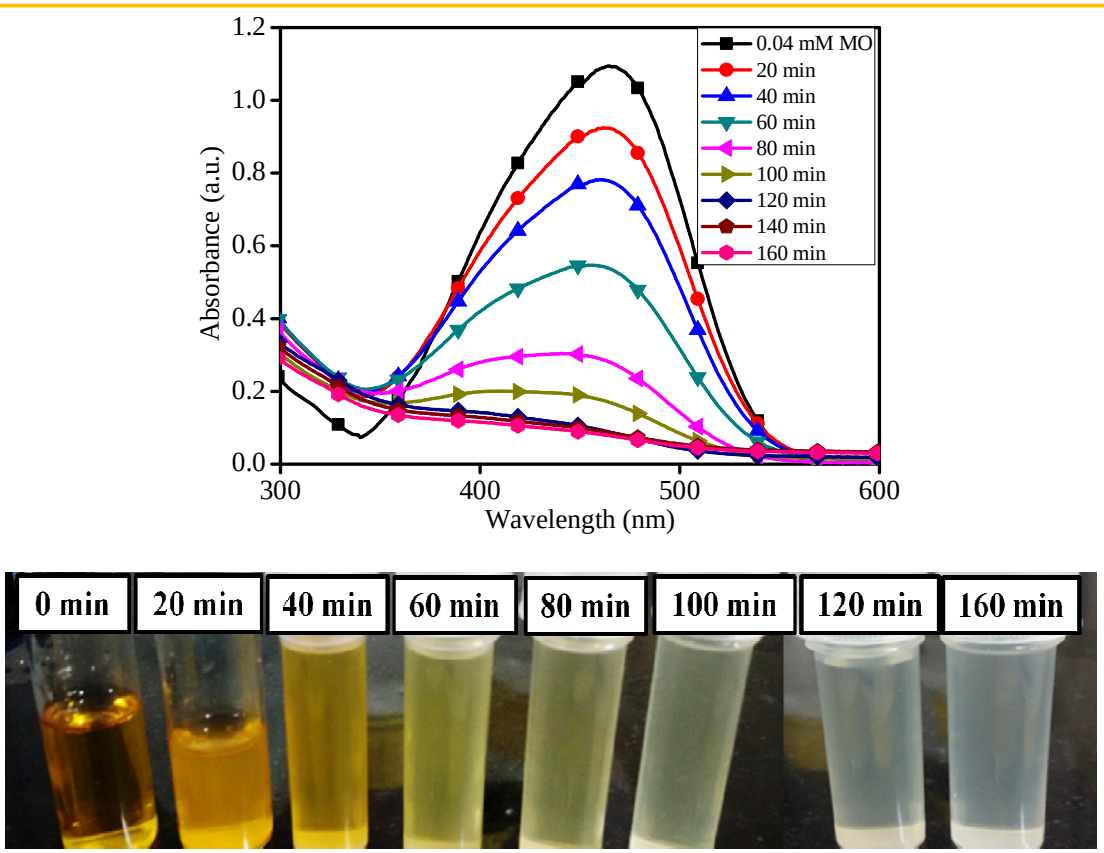

Fig. 24: (a) UV-vis spectrum of photocatalytic degradation of MO using 1wt% Se-ZnS and (b) Decrease in intensity of color of MO with increasing time of UV irradiation

Fig. 24 depicts time-dependent UV-Vis spectrum of photodegradation of 0.04 mM MO solution using 1wt% Se-ZnSNCs during time course of UV irradiation. The spectrum was obtained by scanning in the range of 200-800 nm. The absorption peaks corresponding to dye diminishing and finally disappearing due to the photocatalytic degradation. Wang [90] observed similar declining behaviour of peaks for MO dye using phosphotungstic acid. The spectrum of MO exhibits the main band in the visible region with a maximum at 460 nm. The decrease of absorption peaks of MO at λ_{max} = 460 nm, in Fig. 24(a), indicates that the dye has been degraded. Complete degradation of dye was observed after 160 min. The change in the concentration of MO dye is also confirmed by visible change in the dye color as displayed in Fig. 24(b). The color of the dye diminished gradually from 0 min to 160 min time of UV irradiation.

4.4.5 CO_2 evolution analysis

The complete degradation of MO was further confirmed by measuring the amount of carbon dioxide (CO_2) evolving during the process of photodegradation. Fig. 25a depicts the amount of CO_2 formed during 80 min and 160 min of UV irradiation.

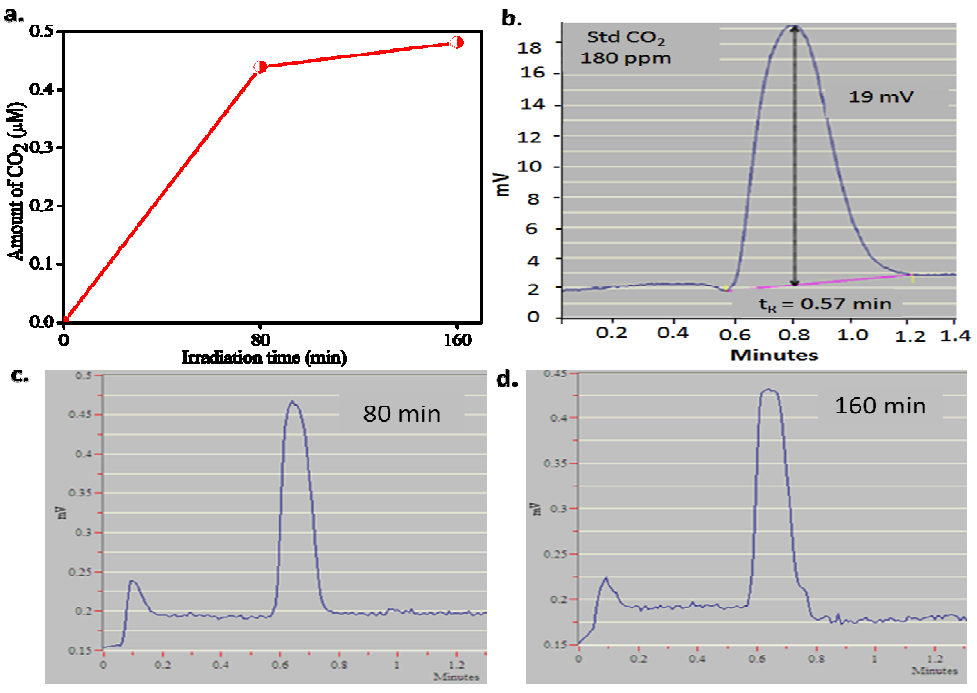

Fig. 25: (a) Amount of CO_2 evolved by 1wt% Se-ZnSNCs at 80 min and 160 min of UV irradiation **(b)** Std of CO_2 180 ppm and **(c-d)** CO_2 evolution after 80 min and 160 min, respectively

It shows the exponential increase in evolution of CO_2 depending on the extent of photocatalytic activity by Se-ZnS photocatalyst. 0.44 µM and 0.48 µM of CO_2 are generated after 80 min and 160 min, respectively of UV irradiation. This indicates that MO has been completely photomineralized into CO_2, H_2O and other simpler inorganic by-products.

4.4.6 Kinetics for photocatalytic degradation

The photooxidation of MO was found to follow pseudo first-order kinetics as observed in Fig. 26a using a simplified Langmuir–Hinshelwood model, r = -dC/dt = k(KC)/(1 + KC) where r is the initial rate of photocatalytic degradation (mol $l^{-1}min^{-1}$), C is the concentration of the reactant (mol l^{-1}), t is the irradiation time (min), k is the rate constant and K is the Langmuir–Hinshelwood adsorption constant (mol^{-1}). At low concentration, KC can be neglected with respect to 1 and a simplified equation can be derived:

$$r = -dC/dt = kKC \text{ or } C/C_0 = e^{-kKt} = e^{-kt} \text{ or } \ln(C/C_0) = -kt$$

where k is the apparent rate constant of the pseudo-first order (min^{-1}) reaction, C_0 is the initial concentration and C is the concentration of MO at time t.

It was found that the rate of photodegradation increased linearly with increasing Se concentration from 0.25wt% to 1wt% and decreased or showed a negligible effect with 2wt% Se-ZnSNCs. The increased degradation rate was probably due to increasing number of trap sites in the Se-ZnS from 0.25wt% to 1wt%, which in turn increased the number of hydroxyl and superoxide radicals. Whereas 2wt% Se loading might have caused the decrease in UV light penetration leading to comparatively less photodegradation efficiency.

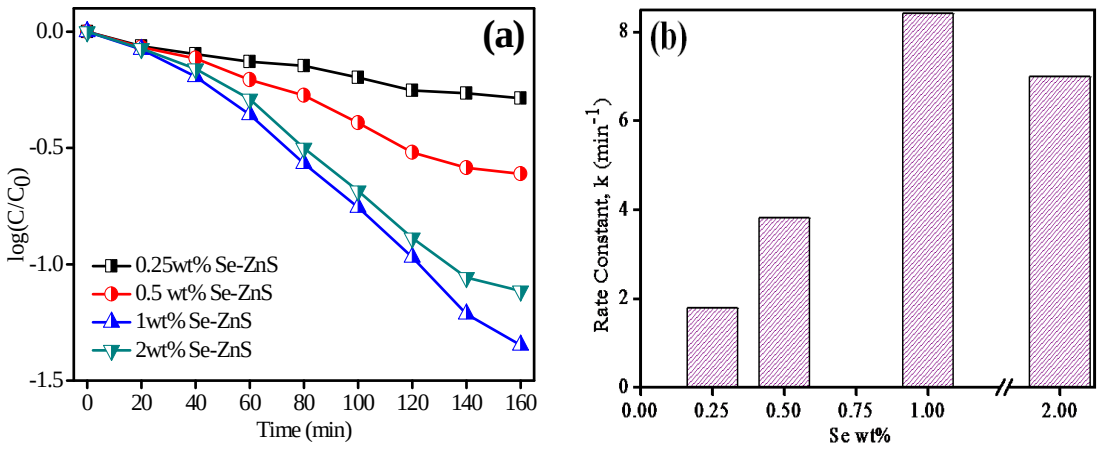

Fig. 26: (a) Kinetic study of MO photodegradation by Se-ZnSNCs and **(b)** variation of rate constant at different Se catalyst concentration (0.25wt%, 0.5wt%, 1wt% and 2wt%)

Rate constant, k (Fig. 26b) was determined from the slope of the linear relationship of the natural logarithm of the ratio between the initial concentration of dye (C_0) and the concentration after photo-catalytic degradation (C) versus the corresponding irradiation time. The k values ca. were $1.79x10^{-3}$, $3.82x10^{-3}$, $8.42x10^{-3}$ and $6.99x10^{-3}$ $min^{-1}$for 0.25wt% Se-ZnS, 0.5wt% Se-ZnS, 1wt% Se-ZnS and 2wt% Se-ZnS, respectively. It indicated that 1wt% Se-ZnS ($8.42x10^{-3}$ min^{-1}) was the optimum concentration for enhancing the activity of ZnS photocatalyst.

Here at the optimal level, Se mainly acted as a charge carrier recombination center. The reason may be assigned to the fact that the recombination rate of the electron-hole pair decreases with the increasing concentration of impregnated material due to increase in number of trap sites. It also causes to the decrease in the average distance between the trap sites due to increase in the number of impregnated molecules confined within a particle [89]. At lower concentrations below the optimal value, photoreactivity increases with an increasing dopant concentration because of available trapping sites. Thus, the appearance of an optimal dopant concentration is a result of the delicate balance of an increase in trap sites leading to efficient trapping and fewer trapped carriers leading to longer lifetimes for interfacial charge transfer.

4.4.7 Mechanism of photocatalysis of MO

On the basis of the previous discussion, the photocatalytic degradation reaction mechanism of MO by Se-ZnSNCs is proposed (Fig. 32). As shown in Fig. 32, the photocatalytic degradation of MO occurs as follows: the first step of photocatalysis is the generation of electron-hole pairs in the ZnS. After absorption of energy equal to or greater than the band gap of the ZnS, the holes (h^+_{VB}) and electrons (e^-_{CB}) are generated in valence band (VB) and conduction band (CB), respectively. The electrons from CB get transferred to co-catalyst SeNPs, while VB holes remain free on the ZnS semiconductor [70]. The transference of excited electrons from ZnS to co-catalyst Se continues until the two systems attain equilibration. This greatly reduces the possibility of electron-hole recombination and resulting in their efficient separation. In the second step, these charge carriers react with absorbed species i.e. photoelectrons reduce the oxygen (O_2) to oxygen radicals ($^{\bullet}O_2^-$), and finally they transform into hydroxyl radicals ($^{\bullet}OH$); in turn, photoinduced holes oxidize the hydroxyl (H_2O) to hydroxyl radicals ($^{\bullet}OH$).

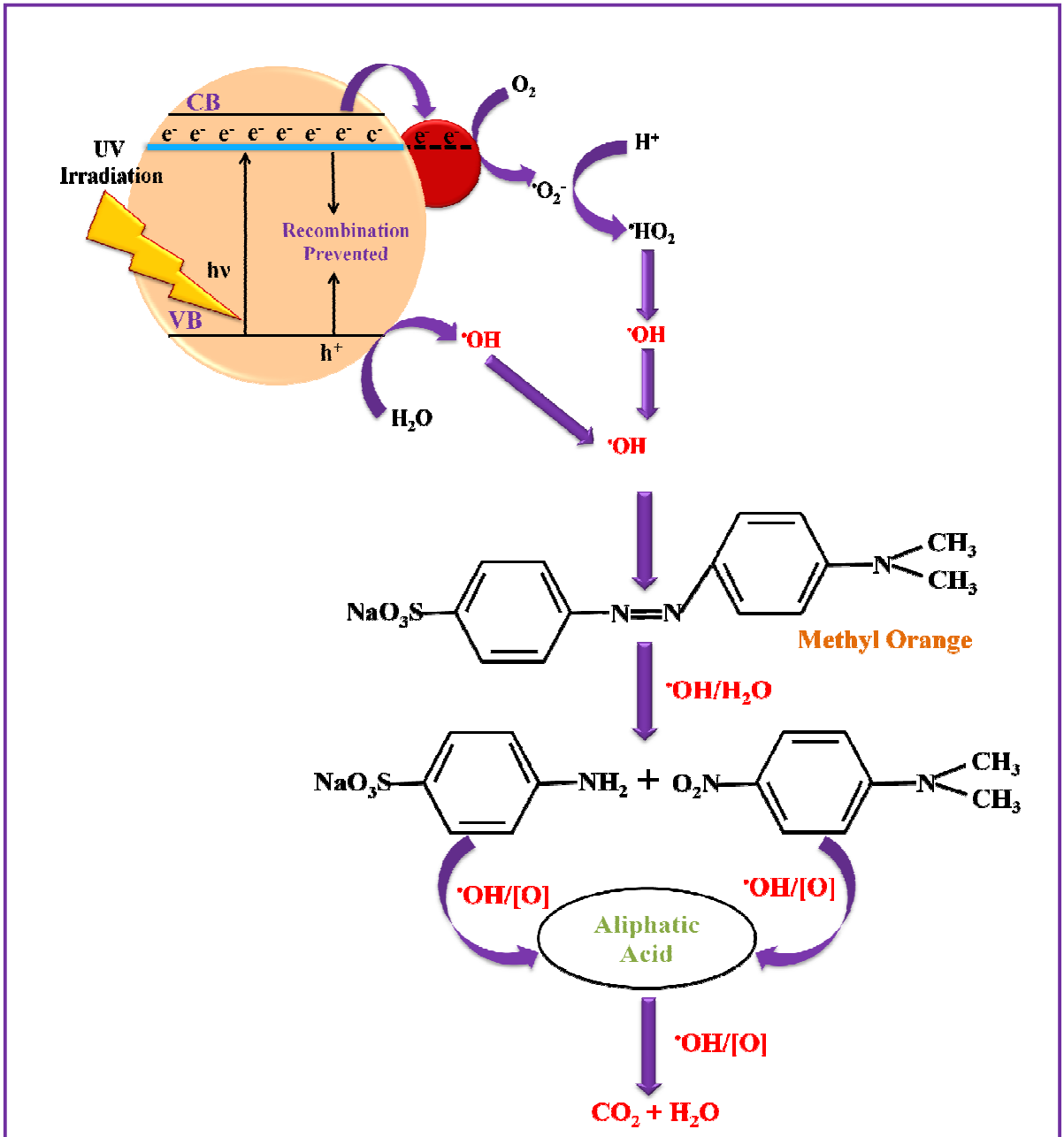

Fig. 27: Schematic representation of mechanism of photocatalysis by Se-ZnSNCs for tuning the rate of photocatalytic reaction of MO degradation under UV irradiation

These hydroxyl radicals ($^{\bullet}OH$) have the ability to decompose methyl orange effectively by attacking on N=N by which the complex dissociates into two intermediates which are presumably unstable in the presence of $^{\bullet}OH$ radical and gets converted to aliphatic acid which is finally break down to produce carbon dioxide (CO_2), water (H_2O) and simpler inorganic by-products.

It can be summed up by saying that at higher concentration 1wt% of impregnated Se, the rate of photocatalytic degradation of organic dye is increased as a result of increase in number of trapping sites in the photocatalyst. SeNPs on the surface of ZnS act as a sink for the photo-generated electrons and reduces the rate of electron-hole pair recombination. It leads to the formation of more number of charge carriers on the surface of the photocatalyst which assist in improved and efficient oxidation of reactant substrates by hydroxyl radical ($^{\bullet}OH$) which are produced by reaction of these charge carriers with absorbed species i.e. O_2 and H_2O. It is a strong oxidant, and determines the overall photocatalytic reaction of the reaction substrate.

Thus, the present study demonstrates (a) the use of biosynthesized Se nanoparticles (SeNPs) as co-catalysts impregnated on ZnS so as generate Se-ZnS nanocomposites (Se-ZnSNCs) with improved photocatalytic efficiency; and (b) application of as-synthesized nanocomposites in UV-based photocatalytic degradation of dye, methyl orange. The study presents a hypothesized mechanism of the photodegradation facilitated by the Se-ZnSNCs.

5. Conclusions

Increasing awareness towards green chemistry and biological processes has led to a desire to develop an eco-friendly and sustainable methods for the synthesis of nanoparticles. We hereby report a green and eco-friendly biological method to synthesize SeNPs by bioreduction of selenite using *Bacillus sp.* at 37°C. Unlike other processes in physical and chemical methods, which involve hazardous chemicals and toxic by-products, microbial biosynthesis of nanoparticles is also cost-effective.

The biosynthesized SeNPs are successfully used as a co-catalyst for enhancing the photocatalytic activity of ZnSNPs. Se impregnated ZnS nanocomposites (0.25wt%, 0.5wt%, 1wt% and 2wt% Se-ZnSNCs) were synthesized by facile wet impregnation method which exhibited enhanced band gap and surface area as compared to bare ZnS. Heterogeneous photocatalysis using these semiconductors offers a green technology for the removal of hazardous compounds present in the industrial effluents and is more efficient than conventional methods. This is because as the photocatalytic process gradually breaks down the contaminant molecules, no residue of the original material remains and therefore no sludge requiring disposal to landfill is produced. The catalyst itself is unchanged during the process and no consumable chemicals are required. This result in considerable savings and a simpler operation of the equipment involved. Additionally, because the contaminant is attracted strongly to the surface of the catalyst, the process will continue to work at very low concentrations.

Kinetics for the degradation of methyl orange by Se-ZnSNCs was studied systematically. From the kinetics of photocatalysis of dye it was observed that photodegrdation of MO followed pseudo first-order kinetics where 0.02 g of 1wt% Se-ZnSNCs showed maximum degradation efficiency of 95% in 160 min under UV irradiation with rate constant (k) value of 8.42×10^{-3} min^{-1}. The impact of enhanced ROS generation was consistent with higher photocatalytic dye degradation as due to impregnation of Se, more trap sites for electrons and holes are generated, more electron-hole pairs are produced and thus causing an increase in the amount hydroxyl radicals and superoxide ions responsible for the degradation of organic pollutant. As a result, the photocatalytic activity of ZnS is increased. Amount of 0.44 µM and 0.48 µM of CO_2 evolved during 80 min and 160 min of UV irradiation confirmed complete photo-mineralization of methyl orange by Se co-catalyzed ZnS photocatalyst.

Thus, the implementation of green synthesis principles for the production of biosynthesized co-catalyst for semiconductor nanoparticles has proved to be effective approach for generation of a heterogeneous photocatalyst that can possibly lead to a great reduction in waste generation, less hazardous chemical synthesis, improved catalysis, and finally an inherently safe environment.

6. References

1. Mansoori, G.A., Soelaiman, T.F. (2005). Nanotechnology- an introduction for the standards community. *Journal of ASTM International*, 2, 1-21.
2. Paull, R., Wolfe, J., Hebert, P., Sinkula, M. (2003). Investing in nanotechnology. *Nature Biotechnology*, 21, 1144-1147.
3. Mansoori, G.A., Bastami, T. R., Ahmadpour, A., Eshaghi, Z. (2008). Environmental application of nanotechnology. *Annual Review of Nano Research*, 2, 439-488.
4. Sabesh, R. (2008). Nanotechnology and environment. *Eco news*, 14, 16.
5. Fujishima, A., Honda, K. (1972). Electrochemical photolysis of water at a semiconductor electrode. *Nature*, 238, 37-38.
6. Rogach, A.L., Talapin, D.V., Weller, H. (2003). Semiconductor nanoparticles, In: *Colloids and Colloid Assemblies: Synthesis, Modification, Organization and Utilization of Colloid Particles.* Wiley-VCH, Germany, pp. 52-91.
7. Ibhadon, A.O., Fitzpatrick, P. (2013). Heterogeneous photocatalysis: Recent advances and applications. *Catalysts*, 3, 189-218.
8. Fang, X., Zhai, T., Gautam, U.K., Li, L., Wu, L., Bando, Y., Golberg, D. (2011). ZnS nanostructures: from synthesis to applications. *Progress in Materials Science*, 56, 175-287.
9. El-Kemary, M., El-Shamy, H. (2009). Fluorescence modulation and photodegradation characteristics of safranin O dye in the presence of ZnS nanoparticles. *Journal of Photochemistry and Photobiology A: Chemistry*, 205, 151-155.
10. Wood, A., Giersig, M., Mulvaney, P. (2001). Fermi level equilibration in quantum dot-metal nanojunctions. *The Journal of Physical Chemistry B*, 105, 8810-8815.
11. Tong, T., Zhang, J., Tian, B., Chen, F., He, D. (2008). Preparation of Fe^{3+} doped TiO_2 catalysts by controlled hydrolysis of titanium alkoxide and study on their photocatalytic activity for methyl orange degradation. *Journal of Hazardous Materials*, 155, 572-579.
12. Andronic, L., Hristache, B., Enesca, A., Visa, M., Duta, A., (2009). Studies on titanium oxide catalyst doped with heavy metals (cadmium, copper and nickel). *Environmental Engineering and Management Journal*, 8, 747-751.

13. Singla, P., Sharma, M., Pandey, O. P., Singh, K. (2014). Photocatalytic degradation of azo dyes using Zn-doped and undoped TiO_2 nanoparticles. *Applied Physics A*, 116, 371-378.
14. Sangpour, P., Hashemi, F., and Moshfegh, A.Z. (2010). Photoenhanced degradation of methylene blue on cosputtered M:TiO_2 (M: Au, Ag, Cu) nanocomposite systems: a comparative study. *The Journal of Physical Chemistry C*, 114, 13955-13961.
15. Lu, N., Zhao, H., Li, J., Quan, X., Chen, S. (2008). Characterization of boron-doped TiO_2 nanotube arrays prepared by electrochemical method and its visible light activity. *Separation and Purification Technology*, 62, 668-673.
16. Pouretedala, H.R., Norozi, A., Keshavarza, M.H., Semnanic, A. (2009). Nanoparticles of zinc sulfide doped with manganese, nickel and copper as nanophotocatalyst in the degradation of organic dyes. *Journal of hazardous materials*, 162, 674-681.
17. Rajabia, H.R., Khani, O., Shamsipur, M., Vatanpour, V. (2013). High-performance pure and Fe^{3+}-ion doped ZnS quantum dots as green nanophotocatalysts for the removal of malachite green under UV-light irradiation. *Journal of Hazardous Materials*, 250, 370-378.
18. Raksha, K.R., Ananda, S., Madegowda, N.M. (2015). Study of kinetics of photocatalysis, bacterial inactivation and •OH scavenging activity of electrochemically synthesized Se^{4+}doped ZnS nanoparticles. *Journal of Molecular Catalysis A: Chemical*, 396, 319-327.
19. Korbekandi, H., Iravani, S., Abbasi, S. (2009). Production of nanoparticles using organisms. *Critical Reviews in Biotechnology*, 29, 279-306.
20. Yan, S., Wang, H., Zhang, Y., Li, S., Xiao, Z. (2009). Direct solution-phase synthesis of Se submicrotubes using selenium powder as selenium source. *Materials Chemistry and Physics*, 114, 300-303.
21. Mondal, K., Roy, P., Srivastava, S.K. (2007). Facile biomolecule-assisted hydrothermal synthesis of trigonal selenium microrods. *Crystal Growth and Design*, 8, 1580-1584.
22. Berger, L. I. (1996). *Semiconductor Materials.* CRC Press, Florida, pp. 86-88.
23. Khataee, A.R., Mirzajani, O. (2010). UV/peroxydisulfate oxidation of CI Basic Blue 3: Modeling of key factors by artificial neural network. *Desalination*, 251, 64-69.
24. Muhd Julkapli, N., Bagheri, S., Bee Abd Hamid, S. (2014). Recent advances in heterogeneous photocatalytic decolorization of synthetic dyes. *The Scientific World Journal*, 2014, 1-25.

25. Pal, B., Pal, B. (2015). Tuning the optical and photocatalytic properties of anisotropic ZnS nanostructures for the selective reduction of nitroaromatics. *Chemical Engineering Journal*, 263, 200-208.
26. Taniguchi, N. (1974). On the basic concept of 'Nano-Technology'. In: *Proceedings of the international conference on production engineering*. Japan Society of Precision Engineering, Tokyo, pp. 18-23.
27. Schmid, G. (2004). *Nanoparticles: from Theory to Applications*. Wiley-VCH, Germany.
28. Nanomaterials. (2013). In: The Essential Chemical Industry Online. The University of York, USA. (www.essentialchemicalindustry.org)
29. Raimondi, F., Scherer, G. G., Kotz, R., Wokaun, A. (2005). Nanoparticles in energy technology: examples from electrochemistry and catalysis. *Angewandte Chemie International Edition*, 44, 2190-2209.
30. Filipponi, L., Sutherland, D. (2010). Fundamental nano-effects. In: *NANOYOU Training Kit in Nanoscience and Nanotechnologies*. European Communities FP7 Training Module. pp. 24.
31. Njoki, P. N., Lim, I.I.S., Mott, D., Park, H.Y., Khan, B., Mishra, S., Sujakumar, R., Luo, J., Zhong, C. J. (2007). Size correlation of optical and spectroscopic properties for gold nanoparticles. *The Journal of Physical Chemistry C*, 111, 14664-14669.
32. Boysen, E., Muir, N.C. (2011). *Nanotechnology for Dummies* (2nd ed.). Wiley-VCH, Germany.
33. Garcia-Torres, J., Gomez, E., Valles, E. (2012). Measurement of the giant magnetoresistance effect in cobalt–silver magnetic nanostructures: Nanowires. *The Journal of Physical Chemistry C*, 116, 12250–12257.
34. Sundaresan, A., Bhargavi, R., Rangarajan, N., Siddesh, U., Rao, C. N. R. (2006). Ferromagnetism as a universal feature of nanoparticles of the otherwise nonmagnetic oxides. *Physical Review B: Condensed Matter and Materials Physics*, 74, 161306_1-161306_4.
35. Kohler, M., Fritzsche, W. (2004). *Nanotechnology: An Introduction to nanostructuring techniques*. Wiley-VCH, Germany, pp. 25-32.
36. Umer, A., Naveed, S., Ramzan, N. (2012). Selection of a suitable method for the synthesis of copper nanoparticles. *Nano*, 7, 1230005_1-1230005_18.

37. Sastry, M., Ahmad, A., Khan, M.I., Kumar, R. (2004). Microbial nanoparticle production. In: Niemeyer, C.M., Mirkin, C.A. (eds), *Nanobiotechnology- Concepts, Applications and Perspectives*. Wiley-VCH, Germany, pp. 126-135.
38. Makarov, V. V., Love, A. J., Sinitsyna, O. V., Makarova, S. S. , Yaminsky, I. V., Taliansky, M. E., Kalinina, N. O. (2014). "Green" nanotechnologies: Synthesis of metal nanoparticles using plants. *Acta Naturae*, 6, 35-44.
39. Arunachalam, K.D., Annamalai, S.K., Hari, S. (2013). One-step green synthesis and characterization of leaf extract-mediated biocompatible silver and gold nanoparticles from *Memecylon umbellatum. International Journal of Nanomedicine*, 8, 1307-1315.
40. Ghosh, S., Patil, S., Ahire, M., Kitture, R., Gurav, D.D., Jabgunde, A.M., Kale, S., Pardesi, K., Shinde, V., Bellare, J., Dhavale, D.D., Chopade, B.A. (2012). *Gnidia glauca* flower extract mediated synthesis of gold nanoparticles and evaluation of its chemocatalytic potential. *Journal of Nanobiotechnology*, 10, 1-17.
41. Zhan, G., Huang, J., Du, M., Abdul-Rauf, I., Ma, Y., Li, Q. (2011). Green synthesis of Au-Pd bimetallic nanoparticles: single-step bioreduction method with plant extract. *Materials Letters*, 65, 2989-2991.
42. Vigneshwaran, N., Ashtaputre, N.M., Varadarajan, P.V., Nachane, R.P., Paralikar, K.M., Balasubramanya, R.H. (2007). Biological synthesis of silver nanoparticles using the fungus *Aspergillus flavus*. *Materials Letters*, 66, 1413-1418.
43. Golinska, P., Wypij, M., Ingle, A.P., Gupta, I., Dahm, H., Rai, M. (2014). Biogenic synthesis of metal nanoparticles from actinomycetes: biomedical applications and cytotoxicity. *Applied Microbiology and Biotechnology*, 98, 8083-8097.
44. Thenmozhi, M., Kannabiran, K., Kumar, R., Khanna, V.G. (2013). Antifungal activity of *Streptomyces sp* VITSTK7 and its synthesized Ag_2O/Ag nanoparticles against medically important Aspergillus pathogens. *Journal of Medical Mycology*, 23, 97-103.
45. Ahmad, A., Senapati, S., Khan, M.I., Kumar, R., Sastry, M. (2003). Extracellular biosynthesis of monodisperse gold nanoparticles by a novel extremophilic actinomycete, *Thermomonospora sp. Langmuir*, 19, 3550-3553.
46. Ahmad, A., Senapati, S., Khan, M.I., Ramani, R., Srinivas, V., Sastry, M. (2003). Intracellular synthesis of gold nanoparticles by a novel alkalotolerant actinomycete, *Rhodococcus species*. *Nanotechnology*, 14, 824-828.

47. Dameron, C.T., Reese, R.N., Mehra, R.K., Kortan, A.R., Carroll, P.J., Steigerwald, M.L., Brus, L.E., Winge, D.R. (1989). Biosynthesis of cadmium sulphide quantum semiconductor crystallites. *Nature*, 338, 596-597.
48. Kowshik, M., Deshmukh, N., Vogel, W., Urban, J., Kulkarni, S.K., Paknikar, K.M. (2002). Microbial synthesis of semiconductor CdS nanoparticles, their characterization, and their use in the fabrication of an ideal diode. *Biotechnology and Bioengineering*, 78, 583-588.
49. Seshadri, S., Saranya, K., Kowshik, M. (2011). Green synthesis of lead sulphide nanoparticles by the lead resistant marine yeast. *Rhodosporidium diobovatum. Biotechnology Progress*, 27, 1464-1469.
50. Kowshik, M., Ashtaputre, S., Kharrazi, S., Vogel, W., Urban, J. (2003). Extracellular synthesis of silver nanoparticles by a silver-tolerant yeast strain MKY3. *Nanotechnology*, 14, 95-100.
51. Mourato, A., Gadanho, M., Lino, A.R., Tenreiro, R. (2011). Biosynthesis of crystalline silver and gold nanoparticles by extremophilic yeasts. *Bioinorganic Chemistry and Applications*, 2011, 1-8.
52. Hulkoti, N.I., Taranath, T.C. (2014). Biosynthesis of nanoparticles using microbes- a review. *Colloids and Surfaces B: Biointerfaces*, 121, 474-483.
53. Vala, A.K. (2014). Intra and extracellular biosynthesis of gold nanoparticles by a marine-derived fungus *Rhizopus oryzae. Synthesis and Reactivity in Inorganic, Metal-Organic, and Nano-Metal Chemistry*, 44, 1243-1246.
54. Yip, J., Liu, L., Wong, K. H., Leung, P. H., Yuen, C. W. M., & Cheung, M. C. (2014). Investigation of antifungal and antibacterial effects of fabric padded with highly stable selenium nanoparticles. *Journal of Applied Polymer Science*, 131, 1-8.
55. Gade, A. K., Bonde, P., Ingle, A. P., Marcato, P. D., Duran, N., Rai, M. K. (2008). Exploitation of *Aspergillus niger* for synthesis of silver nanoparticles. *Journal of Biobased Materials and Bioenergy*, 2, 243-247.
56. Vigneshwaran, N., Ashtaputre, N.M., Varadarajan, P.V., Nachane, R.P., Paralikar, K.M., Balasubramanya, R.H. (2007). Biological synthesis of silver nanoparticles using the fungus *Aspergillus flavus*. *Materials Letters*, 66, 1413-1418.
57. Bharde, A., Rautaray, D., Bansal, V., Ahmad, A., Sarkar, I., Yusuf, S. M., Sanyal, M., Sastry, M. (2006). Extracellular biosynthesis of magnetite using fungi. *Small*, 2, 135-141.

58. Iravani, S. (2014). Bacteria in nanoparticle synthesis: Current status and future prospects. *International Scholarly Research Notices.* 2014, 1-18.
59. Rajalakshmi, M., Arora, A.K. (1999). Optical properties of selenium nanoparticles dispersed in polymer. *Solid State Communications,* 110, 75-80.
60. Jain, R., Gonzalez-Gil, G., Singh, V., Hullebusch, E.V., Farges, F., Lens, N.L.P. (2014). Biogenic Selenium Nanoparticles: Production, Characterization and Challenges. In: Ashok Kumar (ed.) *Biotechnology- Nanobiotechnology*. Studium press LLC, USA, pp. 361-390.
61. Johnson, N.C., Manchester, S., Sarin, L., Gao, Y., Kulaots, I., Hurt, R.H. (2008). Mercury vapor release from broken compact fluorescent lamps and in situ capture by new nanomaterial sorbents. *Environmental Science and Technology*, 42, 5772-5778.
62. Fellowes, J.W., Pattrick, R.A.D., Green, D.I., Dent, A., Lloyd, J.R., Pearce, C.I. (2011). Use of biogenic and abiotic elemental selenium nanospheres to sequester elemental mercury released from mercury contaminated museum specimens. *Journal of Hazardous Materials*, 189, 660-669.
63. Chiou, Y.D., Hsu, Y.J. (2011). Room-temperature synthesis of single-crystalline Se nanorods with remarkable photocatalytic properties. *Applied Catalysis B: Environmental*, 105, 211-219.
64. Yang, L.B., Shen, Y.H., Xie, A.J., Liang, J.J., Zhang, B.C. (2008). Synthesis of Se nanoparticles by using TSA ion and its photocatalytic application for decolorization of cango red under UV irradiation. *Materials Research Bulletin*, 43, 572-582.
65. Nath, S., Ghosh, S.K., Panigahi, S., Thundat, T., Pal, T. (2004). Synthesis of selenium nanoparticle and its photocatalytic application for decolorization of methylene blue under UV irradiation. *Langmuir,* 20, 7880-7883.
66. Hu, J.S., Ren, L.L., Guo, Y.G., Liang, H.P., Cao, A.M., Wan, L.J., Bai, C.L. (2005). Mass production and high photocatalytic activity of ZnS nanoporous nanoparticles. *Angewandte Chemie*, 117, 1295-1299.
67. Muruganandham, M., Amutha, R., Repo, E., Sillanpää, M., Kusumoto, Y., Abdulla-Al-Mamun, M.D. (2010). Controlled mesoporous self-assembly of ZnS microsphere for photocatalytic degradation of methyl orange dye. *Journal of Photochemistry and Photobiology A: Chemistry*, 216, 133-141.
68. Beydoun, D., Amal, R., Low, G., McEvoy, S. (1999). Role of nanoparticles in photocatalysis. *Journal of Nanoparticle Research*, 1, 439-458.

69. Vinu, R., Madras, G. (2012). Environmental remediation by photocatalysis. *Journal of the Indian Institute of Science*, 90, 189-230.
70. Yang, J., Wang, D., Han, H., Li, C. (2013). Roles of cocatalysts in photocatalysis and photoelectrocatalysis. *Accounts of Chemical Research*, 46, 1900-1909.
71. Reddy, R.K., Nakata, K., Ochiai, T., Murakami, T., Tryk, D.A., Fujishima, A. (2011). Facile fabrication and photocatalytic application of Ag nanoparticles-TiO_2 nanofiber composites. *Journal of Nanoscience and Nanotechnology*, 11, 3692–3695.
72. Pal, B., Singh, R., Singla, S. (2013). Effect of Au and Pt deposition and thermal treatment on the photocatalytic activity of as-prepared ZnS nanorod. *International Journal of Nanoscience*, 12, 1-8.
73. He, L., Freeman, H. S., Lu, L., Zhang, S. (2011). Spectroscopic study of anthraquinone dye/amphiphile systems in binary aqueous/organic solvent mixtures. *Dyes & Pigments*, 91, 389-395.
74. Xu, Y.J., Zhuang, Y., Fu, X. (2010). New insight for enhanced photocatalytic activity of TiO_2 by doping carbon nanotubes: a case study on degradation of benzene and methyl orange. *The Journal of Physical Chemistry C*, 114, 2669–2676.
75. Saha, S., Wang, J.M., Pal, A. (2012). Nano silver impregnation on commercial TiO_2 and a comparative photocatalytic account to degrade malachite green. *Separation and Purification Technology*, 89, 147-159.
76. Hassan, M. S., Amma, T., Khil, M.S. (2014). Synthesis of high aspect ratio $CdTiO_3$ nanofibers via electrospinning: characterization and photocatalytic activity. *Ceramics International*, 40, 423-427.
77. Robinson, T., McMullan, G., Marchant, R., Nigam, P. (2001). Remediation of dyes in textile effluent: a critical review on current treatment technologies with a proposed alternative. *Bioresource Technology*, 77, 247-255.
78. Selvin, R., Hsu, H.L., Arul, N.S., Mathew, S. (2010). Comparison of photo-catalytic efficiency of various metal oxide photo-catalysts for the degradation of methyl orange. *Science of Advanced Materials*, 2, 58-63.
79. Dua, P., Shangandb, X.L., Li, C.H. (2014). Effective photocatalytic degradation of methyl orange utilizing ZnS/TiO2/Chitosan films under simulated solar irradiation. *Applied Mechanics and Materials*, 675, 520-523.
80. Eyasu, A., Yadav, O.P., Bachheti, R.K. (2013). Photocatalytic degradation of methyl orange dye using Cr-doped ZnS nanoparticles. *International Journal of ChemTech Research*, 5, 1452-1461.

81. Chen, D., Huang, F., Ren, G., Li, D., Zheng, M., Wang, Y., Lin, Z. (2010). ZnS nano-architectures: photocatalysis, deactivation and regeneration. *Nanoscale*, 2, 2062-2064.
82. Li, S., Shen, Y., Xie, A., Yu, X., Zhang, X., Yang, L., & Li, C. (2007). Rapid, room-temperature synthesis of amorphous selenium/protein composites using Capsicum annuum L extract. *Nanotechnology*, 18, 1-9.
83. Tam, K., Ho, C.T., Lee, J.H., Lai, M., Chang, C.H., Rheem, Y., Chen, W., Hur, H.G., Myung, N.V. (2010). Growth mechanism of amorphous selenium nanoparticles synthesized by *Shewanella sp*. HN-41. *Bioscience, Biotechnology, and Biochemistry*, 74, 696–700.
84. Lin, Z. H., Wang, C. C. (2005). Evidence on the size-dependent absorption spectral evolution of selenium nanoparticles. *Materials Chemistry and Physics*, 92, 591-594.
85. Kaur, G., Iqbal, M., Bakshi, M.S. (2009). Biomineralization of fine selenium crystalline rods and amorphous spheres. *The Journal of Physical Chemistry C*, 113, 13670–13676.
86. Ji, L. W., Hsiao, Y. J., Tang, I. T., Meen, T. H., Liu, C. H., Tsai, J. K., Wu, T.C., Wu, Y. S. (2013). Annealing effect and photovoltaic properties of nano-ZnS/textured p-Si heterojunction. *Nanoscale Research Letters*, 8, 1-6.
87. Chen, T., Zheng, Y., Lin, J. M., Chen, G. (2008). Study on the photocatalytic degradation of methyl orange in water using Ag/ZnO as catalyst by liquid chromatography electrospray ionization ion-trap mass spectrometry. *Journal of the American Society for Mass Spectrometry*, 19, 997-1003.
88. Gurkan, Y. Y., Kasapbasi, E., Cinar, Z. (2013). Enhanced solar photocatalytic activity of TiO_2 by selenium (IV) ion-doping: characterization and DFT modeling of the surface. *Chemical Engineering Journal*, 214, 34-44.
89. Singla, P., Sharma, M., Pandey, O. P., Singh, K. (2014). Photocatalytic degradation of azo dyes using Zn-doped and undoped TiO2 nanoparticles. *Applied Physics A*, 116, 371-378.
90. Weiping, W., Shuijin, Y. (2010). Photocatalytic degradation of organic dye methyl orange with phosphotungstic acid. *Journal of Water Resource and Protection*, 2, 979-983.